Neural hierarchical models of ecological populations

Maxwell B. Joseph
Earth Lab
Cooperative Institute for Research in Environmental Sciences
University of Colorado Boulder
Boulder, CO 80303, USA
maxwell.b.joseph@colorado.edu

Abstract

Neural networks are increasingly being used in science to infer hidden dynamics of natural systems from noisy observations, a task typically handled by hierarchical models in ecology. This paper describes an emergent class of hierarchical models parameterized by neural networks — neural hierarchical models — and develops a case study with bird populations in the United States. The derivation of such models is outlined beginning with the relationship between linear regression and neural networks, and analogously between a hierarchical ecological model (a dynamic occupancy model), and its neural counterpart. The resulting neural hierarchical model, trained on millions of detection/non-detection time series for hundreds of species, provides insights into colonization and extinction at a continental scale. The model also demonstrates good quantitative predictive performance and reasonable qualitative results about range shifts and macroecological patterns of population persistence at range boundaries. Flexible models are increasingly needed that scale to large data and represent ecological processes. Neural hierarchical models satisfy this need, providing a bridge between deep learning and ecological modeling that combines the function representation power of neural networks with the inferential capacity of hierarchical models.

Introduction

Deep neural networks have proved useful in myriad tasks due their ability to represent complex functions over structured domains (LeCun *et al.* 2015). While ecologists are beginning to use such approaches, e.g., to identify animals in camera trap images (Norouzzadeh *et al.* 2018), there has been relatively little integration of deep neural networks in ecological models of population dynamics.

Ecological dynamics that regulate populations are difficult to observe, and inference often proceeds by modeling the relationship between imperfect data and latent quantities or processes of interest with hierarchical models (Wikle 2003). For example, occupancy models estimate the presence or absence of a species using imperfect detection data (MacKenzie *et al.* 2002), and "dynamic" occupancy models estimate extinction and colonization dynamics (MacKenzie *et al.* 2003). Population growth provides another example, motivating hierarchical models that link noisy observations to mechanistic models (De Valpine & Hastings 2002). In such models, it is often desirable to account for heterogeneity among sample units (e.g., differences among habitats and survey conditions), to better understand ecological dynamics.

Many hierarchical models in ecology account for heterogeneity among sample units using a linear combination of covariate values, despite there often being reasons to expect non-linearity (Lek *et al.* 1996; Austin 2002; Oksanen & Minchin 2002). A variety of solutions exist to account for non-linearity. For example, Gaussian processes have been used for species distribution models (Latimer *et al.* 2009; Golding & Purse 2016), in animal movement models (Johnson *et al.* 2008),

and in point process models for distance sampling data (Johnson *et al.* 2010; Yuan *et al.* 2017). Generalized additive models also have been used to account for spatial autocorrelation (Miller *et al.* 2013; Webb *et al.* 2014), nonlinear responses to habitat characteristics (Knapp *et al.* 2003; Bled *et al.* 2013), and differential catchability in capture-recapture studies (Zwane & Van der Heijden 2004).

Machine learning provides additional tools for approximating potentially nonlinear functions in hierarchical models. For example, Hutchinson *et al.* (2011) combined a site-occupancy model with an ensemble of decision trees to predict bird occurrence, combining a structured observation and process model from ecology with a flexible random forest model. Similar hybrid approaches could be developed for other classes of ecological models and/or machine learning methods. Neural networks seem particularly worthy of attention, given their successful applications in other domains (LeCun *et al.* 2015).

Neural networks have been used in ecology to model observations of populations, but to date have not been integrated into hierarchical models that explicitly distinguish between ecological processes and imperfect observations. For example, neural networks have been used to model the observed abundance of aquatic organisms, but without distinguishing observed from true abundance (Chon *et al.* 2001; Jeong *et al.* 2001, 2008; Malek *et al.* 2012). Neural networks also have been used to model stock-recruitment and apparent presence/absence data (Manel *et al.* 1999; Chen & Hare 2006; Özesmi *et al.* 2006; Harris 2015; Chen *et al.* 2016), but have not yet been extended to account for imperfect detection, despite increasing recognition of its importance (Guillera-Arroita 2017; Tobler *et al.* 2019). Notably, standard neural networks that classify or predict data are of limited use for ecological applications where the data tend to be imperfect, and the primary goal is learning about the dynamics of hard to observe systems. As a solution, this paper describes neural hierarchical models that combine the function representation capacity of neural networks with hierarchical models that represent ecological processes.

Related work

Neural networks

Neural networks are function approximators. Linear regression is a special case, where x is mapped to a predicted value y:

$$y = w^T x,$$

where w is a parameter vector (Fig. 1a). Predicted values are linear combinations of the inputs x due to the product $w^T x$, which restricts the complexity of the mapping from x to y.

Instead of modeling outputs as linear functions of x, a model can be developed that is a linear function of a nonlinear transformation of x. A nonlinear transformation can be specified via polynomial terms, splines, or another basis expansion (Hefley *et al.* 2017), but neural networks parameterize the transformation via a set of sequential hidden layers (Goodfellow *et al.* 2016).

In a neural network with one hidden layer, the first hidden layer maps the length D input x to a length $D^{(1)}$ vector of "activations" $a^{(1)} = W^{(1)}x$, where $W^{(1)}$ is a $D^{(1)} \times D$ parameter matrix. The activations are passed to a differentiable nonlinear activation function g to obtain the "hidden units" of the first layer $h^{(1)} = g(a^{(1)})$ (Fig. 1b).

The final layer of a neural network maps the last hidden layer to an output. For a neural network with one hidden layer, if the output variable y is a K dimensional vector, the output unit activations are given by $a^{(2)} = W^{(2)}h^{(1)}$, where $W^{(2)}$ is a $K \times D^{(1)}$ parameter matrix. The output activation can be written as the composition of functions that transform the inputs x:

$$a^{(2)} = W^{(2)}\Big(g(W^{(1)}x)\Big).$$

Written this way, it is apparent that linear regression is a special case of a neural network with zero hidden layers. Similar to link functions in generalized linear models, outputs can be transformed by an output activation function. For example, if y is unbounded, the identity function can act as an

output activation so that $y = a^{(2)}$. Neural networks that predict probabilities typically use a sigmoid (inverse logit) activation function.

Neural networks usually are trained using stochastic gradient based optimization to minimize a loss function, e.g., the negative log likelihood of a Gaussian distribution for a regression task, a Bernoulli distribution for binary classification, or a Poisson distribution for a count model. Partial derivatives of the model parameters are computed with respect to the loss value via backpropagation, and parameters are updated to reduce the loss. In practice, these partial derivatives are often computed via automatic differentiation over a "mini-batch" of samples, which provides a noisy estimate of the gradient (Ruder 2016).

Neural networks are popular both because of their practical successes in a wide variety of applications, and because they possess some desirable theoretical properties. A neural network with suitable activation functions and a single hidden layer containing a finite number of neurons can approximate nearly any continuous function on a compact domain (Cybenko 1989; Hornik 1991). "Deep" neural networks with many sequential hidden layers also possess desirable theoretical properties for function representation (Lu *et al.* 2017). The field of deep learning, which applies such networks, provides a variety of network architectures to account for temporal structure (Hochreiter & Schmidhuber 1997), spatial structure on regular grids (Long *et al.* 2015), or graphs (Niepert *et al.* 2016), sets of unordered irregular points (Li *et al.* 2018), and spatiotemporal data on grids or graphs (Xingjian *et al.* 2015; Jain *et al.* 2016).

The potential for deep learning has been recognized in Earth science (Reichstein *et al.* 2019), the natural sciences (Ching *et al.* 2018; Gazestani & Lewis 2019; Roscher *et al.* 2019), physical sciences (Carleo *et al.* 2019), chemical sciences (Butler *et al.* 2018), and ecology (Christin *et al.* 2018; Desjardins-Proulx *et al.* 2019). For example, models of lake temperature that combine neural networks with loss functions consistent with known physical mechanisms perform better than physical models and neural networks applied alone (Karpatne *et al.* 2017). Similarly, generative adversarial networks with loss functions that encourage mass-balance have expedited electromagnetic calorimeter data generation from the Large Hadron Collider (Paganini *et al.* 2018; Radovic *et al.* 2018). Convolutional neural networks also have been successfully deployed in population genetics to make inferences about introgression, recombination, selection, and population sizes (Flagel *et al.* 2018). In ecology, hierarchical models present an opportunity to develop similar science-based deep learning methods (Wikle 2019).

Hierarchical models

Hierarchical models combine a data model, a process model, and a parameter model (Berliner 1996; Wikle 2003). Data models represent the probability distribution of observations conditioned on a process and some parameters, e.g., the probability of capturing a marked animal, given its true state (alive or dead). Process models represent probability distribution of the states and their dynamics, conditioned on some parameters. State variables are often incompletely observed, e.g., whether an individual animal is alive or whether a site is occupied. Parameter models represent probability distributions for unknown parameters - priors in a Bayesian framework. In a non-Bayesian setting, parameters are treated as unknowns and estimated from the data, but parameter uncertainty is not represented using probability distributions (Cressie *et al.* 2009).

Neural hierarchical models

Neural hierarchical models are hierarchical models in which the observation, process, or parameter model is parameterized by a neural network. These models are hierarchical (sensu Berliner (1996)) if they distinguish between a modeled process and available data, e.g., between partial differential equations and noisy observations of their solutions (Raissi 2018). "Deep Markov models" - hidden Markov models parameterized by neural networks - provide an example, with successful applications in polyphonic music structure discovery, patient state reconstruction in medical data, and time series forecasting (Krishnan *et al.* 2017; Rangapuram *et al.* 2018). State-space neural networks that use recurrent architectures provide another example dating back two decades (Zamarreño & Vega 1998; Van Lint *et al.* 2002). This class of models inherits the flexibility and scalability of neural networks, along with the inferential power of hierarchical models, but applications in ecology and environmental science are only just beginning to emerge (Wikle 2019).

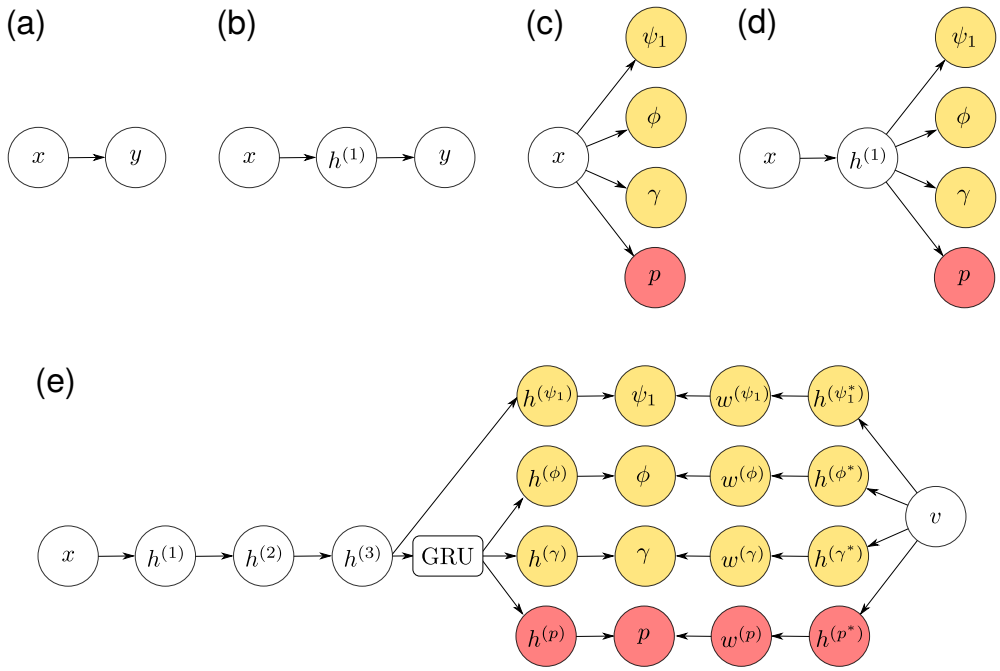

Figure 1: Computation graphs for (a) linear regression, (b) a neural network with one hidden layer, (c) a dynamic occupancy model, (d) a single species neural dynamic occupancy model, and (e) a deep multi-species neural dynamic occupancy model with species embeddings. Yellow and red indicate quantities specific to process and observation components respectively. Inputs are represented by x, and predicted values in panels (a) and (b) by y. Hidden layers are represented by h, with layer-specific superscripts. Outputs include initial occupancy (ψ_1), persistence (ϕ), colonization (γ), and detection (p) probabilities. Latent species embedding vectors are represented by v, and GRU indicates a gated recurrent unit.

Construction of such models from existing hierarchical models is straightforward. One can propose neural variants of occupancy models (MacKenzie *et al.* 2002), dynamic occupancy models (MacKenzie *et al.* 2003; Royle & Kéry 2007), N-mixture models (Royle 2004), mark-recapture models (Jolly 1965; Calvert *et al.* 2009), and other hidden Markov models (Patterson *et al.* 2009; Langrock *et al.* 2012). Output activation functions can be determined from inverse link functions, e.g., sigmoid (inverse logit) activations for probabilities, and loss functions can be constructed from the negative log likelihoods (see Appendix S1 in Supporting Information for example model specifications). To provide a concrete use case, a neural dynamic occupancy model is developed for extinction and colonization dynamics of North American bird communities.

Case study

The North American Breeding Bird Survey (BBS) is a large-scale annual survey aimed at characterizing trends in roadside bird populations (Link & Sauer 1998; Sauer & Link 2011; Sauer *et al.* 2013; Pardieck *et al.* 2018). Thousands of routes are surveyed once a year during the breeding season. Surveys consist of volunteer observers that stop 50 times at points 800 meters apart on a transect, and record all birds detected within 400 meters for three minutes. Species can be present, but not detected, and may go locally extinct or colonize new routes from year to year, motivating the development of dynamic occupancy models which use imperfect detection data to estimate latent presence or absence states (MacKenzie *et al.* 2003; Royle & Kéry 2007).

This case study uses BBS data from 1997-2018 excluding unidentified or hybrid species, restricting the analysis to surveys which meet the official BBS criteria (Pardieck *et al.* 2018). The resulting

data consists of 647 species sampled at 4,540 routes, for a total of 59,384 surveys (not every route is surveyed in each year), 2,969,200 stops, and 38,421,448 detection/non-detection observations.

Process model

A multi-species dynamic occupancy model for spatially referenced routes $s = 1, ..., S$, surveyed in years $t = 1, ...T$, for species $j = 1, ..., J$ aims to estimate colonization and extinction dynamics through time. The true occupancy state $z_{t,s,j} = 1$ if species j is present, and $z_{t,s,j} = 0$ if species j is absent. The model represents $z_{t,s,j}$ as a Bernoulli distributed random variable, where $\Pr(z_{t,s,j} = 1) = \psi_{t,s,j}$. The probability of occurrence on the first timestep is $\psi_{t=1,s,j}$. Subsequent dynamics are determined by probabilities of persistence from time t to $t + 1$ denoted $\phi_{t,s,j}$, and probabilities of colonization from time t to $t + 1$ denoted $\gamma_{t,s,j}$, so that the probability of occurrence in timesteps $t = 2, ..., T$ is (MacKenzie *et al.* 2003):

$$\psi_{t,s,j} = z_{t-1,s,j}\phi_{t-1,s,j} + (1 - z_{t-1,s,j})\gamma_{t-1,s,j}.$$

Observation model

Let $y_{t,s,j}$ represent the total number of stops at which species j was detected in year t on route s. Conditional on a species being present, it is detected at each stop with probability $p_{t,s,j}$. Assume that there are no false-positive detections, so that if a species is absent, it cannot be detected (but see Royle & Link 2006). With $k = 50$ replicate stops on each transect, the observations can be modeled using a Binomial likelihood for one species-route-year combination:

$$[y_{t,s,j} \mid z_{t,s,j}, p_{t,s,j}] = \text{Binomial}(y_{t,s,j} \mid z_{t,s,j}p_{t,s,j}, k),$$

where square brackets denote the probability function. The joint likelihood corresponds to the product of these terms for all years, routes, and species (Dorazio *et al.* 2010).

Parameter models

Heterogeneity in parameter values among routes, years, species, and surveys was represented differently in three models of increasing complexity: a baseline model that maps input features to parameters with a linear combination on the logit scale (MacKenzie *et al.* 2003), a single-species neural hierarchical model that maps inputs to parameters using a neural network with one hidden layer, and a multi-species deep neural hierarchical model (Fig. 1c-e). For all models, input features included Environmental Protection Agency (EPA) level one ecoregions, the first eight principal components of the standard 19 WorldClim Bioclimatic variables averaged across the years 1970-2000, computed for the coterminous United States (Fick & Hijmans 2017), BBS route spatial coordinates, distance from the coast, elevation, and road density within 10 km from the Global Roads Inventory Project (Meijer *et al.* 2018). The model of detection probabilities additionally included survey-level features including temperature, duration, wind, and air conditions.

The neural hierarchical model architectures were motivated by joint species distribution models in which species load onto a shared set of latent factors (Thorson *et al.* 2015, 2016; Warton *et al.* 2015; Ovaskainen *et al.* 2016; Tikhonov *et al.* 2017), and by recent work on deep neural basis expansions (McDermott & Wikle 2019; Wikle 2019). Analogously, the neural networks combined inputs into a latent vector for each route via a series of hidden layers, which is then passed as inputs to hidden layers associated with initial occupancy, colonization, extinction, and detection probabilities. These hidden layers act as latent factors, mapped via a loading matrix to process and observation parameters.

The architecture of the multi-species neural dynamic occupancy model additionally built upon previous work on deep multi-species embedding (Chen *et al.* 2016) and encoder-decoder architectures used in sequence to sequence translation (Sutskever *et al.* 2014). Route-level features were encoded via a series of hidden layers, then passed to a recurrent neural network that decodes a multivariate time series of latent vectors associated with colonization, persistence, and detection (Chung *et al.* 2014). An entity embedding was constructed for each species that combined information among species within genera, families, and orders, and a neural network parameterized species-specific weights for each latent spatiotemporally referenced route feature. The dot product of species-specific

weights and latent spatiotemporal route features generated values for colonization, persistence, and detection probabilities. For additional details, see Appendix S2 in Supporting Information.

Model evaluation

To facilitate predictive performance comparisons, EPA level two ecoregions were randomly assigned to training, validation, and test sets with equal probability (Roberts *et al.* 2017). This resulted in 2154 training routes, 950 validation routes, and 1436 test routes. Training routes were used for parameter estimation, and validation routes were used to select the best performing model based on validation set log-likelihood. The best performing model was retrained using the training and validation data, and the withheld test set routes were used to estimate predictive performance of the final model (Russell & Norvig 2016). Predictive performance was evaluated by computing 95% prediction interval coverage of test set counts, and the area under the receiver operator characteristic curve (AUC) for binarized detection data. For the AUC analysis, cases were taken to be detections $y_{t,s,j} > 0$ and controls were non-detections $y_{t,s,j} = 0$. Predicted test set observation probabilities were constructed via marginalization over latent states so that $\Pr(y_{t,s,j} = 0 \mid p_{t,s,j}, \psi_{t,s,j}) = 1 - \psi_{t,s,j} + \psi_{t,s,j}(1 - p_{t,s,j})^{50}$. Predicted occupancy probabilities for withheld test set routes were computed recursively following MacKenzie *et al.* (2003).

Predictions from final model were qualitatively evaluated to see whether they are plausible, given previous work. The most likely occupancy states were computed at all BBS routes for each year and species (Viterbi 1967), which were then used to compute finite sample population growth rates for each species (Royle & Kéry 2007). To quantify range shifts, annual spatial centroids were computed for each species among routes that were predicted to be occupied (hereafter referred to as "BBS range centroids" to differentiate from the actual centroid of a species' entire range). To evaluate whether the results were consistent with previous findings that population persistence probabilities are highest in the center of a species' range, correspondence between BBS range centroids and persistence probabilities were also assessed using linear regression (Mehlman 1997; Royle & Kéry 2007). These qualitative analyses only used BBS routes surveyed in every year, and species that occurred in all years and at 100 or more routes to avoid bias associated with recently added Canadian routes, and variance associated with rare species (Sauer *et al.* 2017).

Finally, to facilitate interpretation of the final model, additional analyses were performed that provide insight into how the model represented BBS routes and bird species. First, route-level features were visualized using t-distributed stochastic neighbor embedding, which maps high dimensional vectors to lower dimensional representations (Maaten & Hinton 2008). In this lower dimensional space, routes with similar embeddings are close together, and routes with dissimilar embeddings appear distant. By mapping original inputs into this lower dimensional space, it is possible to evaluate how model inputs relate to latent representations (Rauber *et al.* 2016). Second, species' loading vectors, which described how spatiotemporal route features are weighted by process and observation parameters, were compared in terms of cosine similarity, which measures the orientation of loading vectors in latent space, with the expectation that species' occupancy will be positively related if loading vectors are oriented similarly.

Results

The multi-species neural hierarchical model performed best on the withheld validation routes, with a difference in mean validation set negative log likelihood of 6.016 relative to the baseline model and 3.019 relative to the single-species neural hierarchical model. For the final model, 95% prediction interval coverage for observed counts at withheld test set routes was 93.6%, with a standard deviation of 1.6%, a minimum of 85.8%, and a maximum of 97.2%. The model also predicted whether species would be detected on test set routes fairly well, with a mean test set AUC of 0.957, an among-route standard deviation of 0.029, a minimum of 0.722, and a maximum of 0.994 (Fig. 2).

Qualitative results related to range shifts and population growth rates were plausible given previous work. The model identified the invasive Eurasian Collared-Dove (*Streptopelia decaocto*) as having the greatest range centroid displacement from 1997 to 2018 and the highest finite sample population growth rate (Fig. 3), consistent with its invasion of North America from Florida following its introduction in the 1980's (Bled *et al.* 2011). Increasing trends also have previously been reported for the species with the next three highest population growth rates: Bald Eagle (*Haliaeetus leucocephalus*), Wild Turkey (*Meleagris gallopavo*), and Broad-Winged Hawk (*Buteo platypterus*) (Sauer *et al.* 2013).

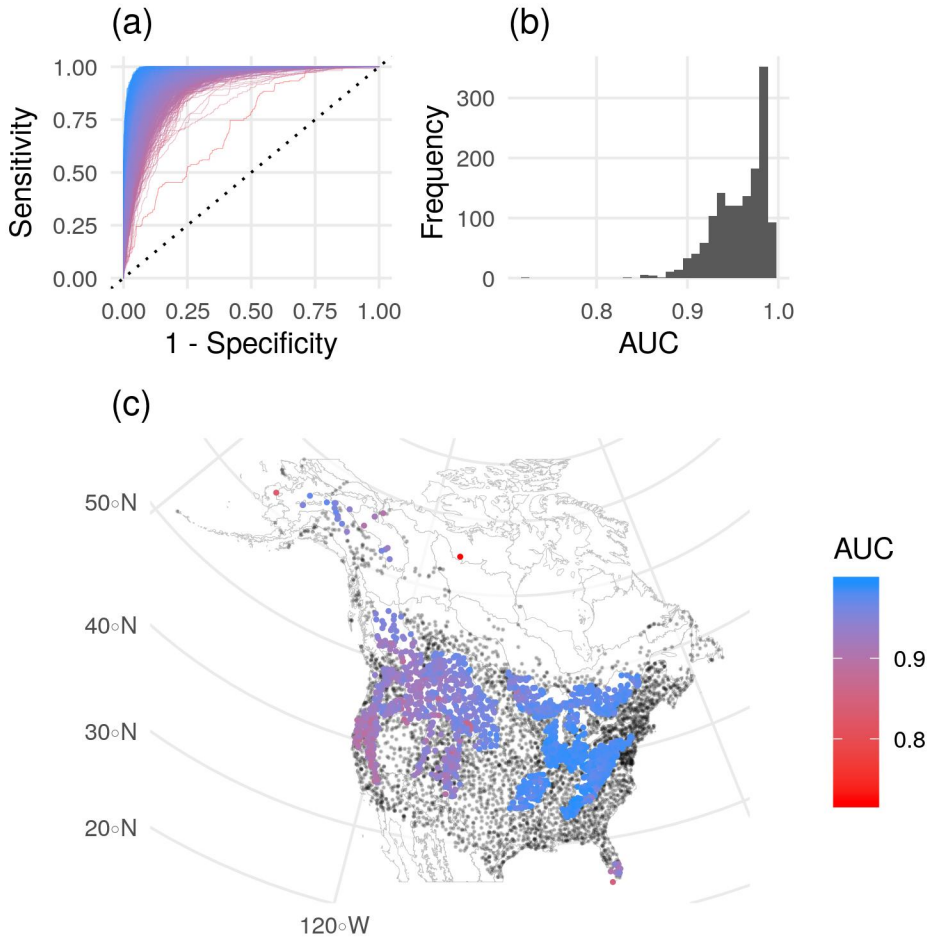

Figure 2: (a) Receiver operator characteristic curves of binarized detection/non-detection data for each survey route in the test set, colored by the area under the curve (AUC). Here, the x-axis is the complement of specificity: the ratio of the number of false positives (incorrectly predicted detections, with no observed detections) to the sum of false positives and true negatives (correctly predicted non-detections with observed non-detections). The y-axis is true positive rate: the ratio of the number of true positives (correctly predicted detections with observed detections) to the sum of true positives and false negatives (incorrectly predicted non-detections with observed detections). The overall distribution of AUC values is shown in (b), and (c) shows the locations of test set routes colored by AUC values, where black dots represent routes that were used to train the final model.

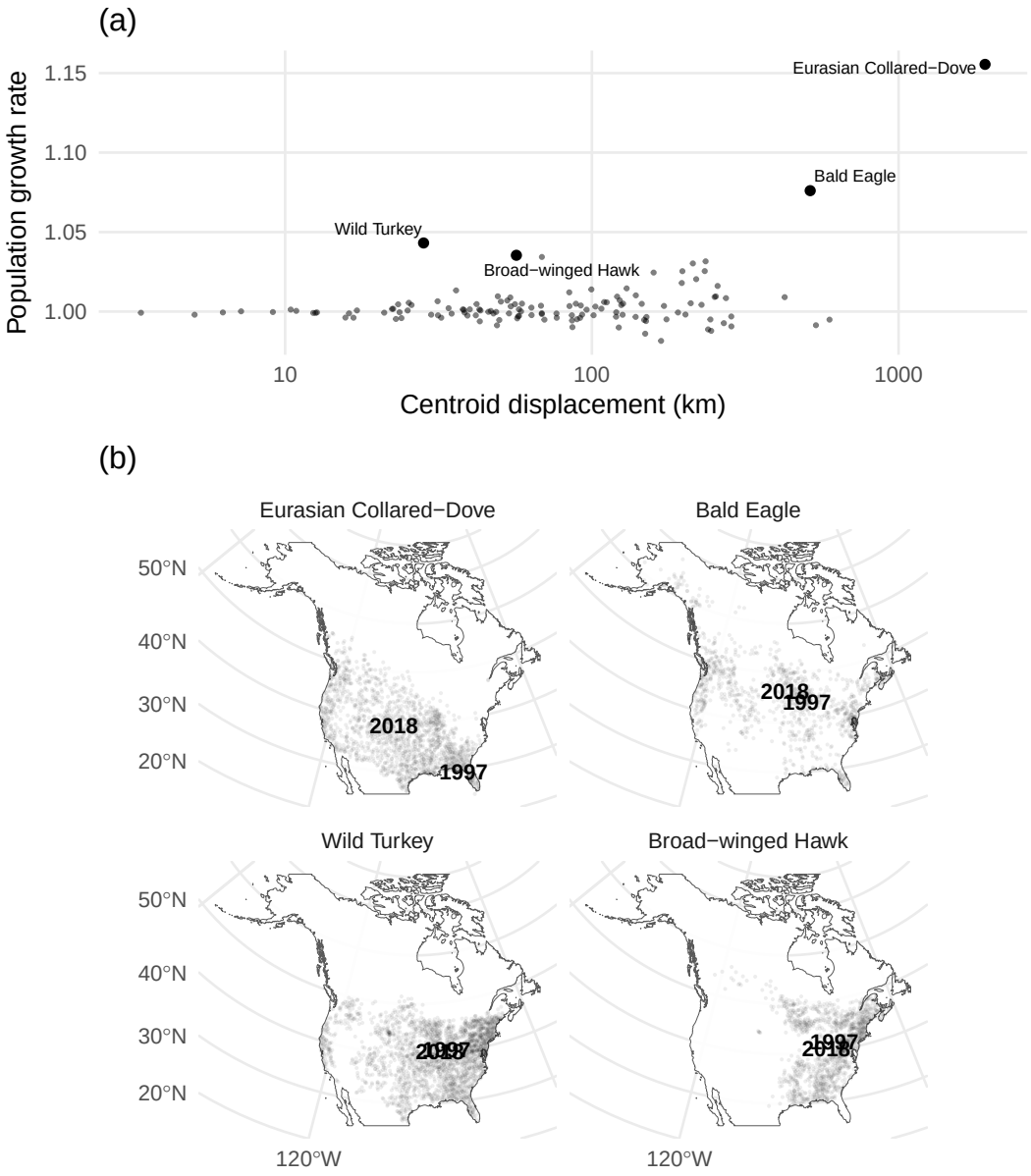

Figure 3: (a) Scatter plot relating the centroid displacement of bird species (x-axis) from 1997 to 2018 in kilometers to finite-sample growth rate (y-axis), where a growth rate of 1 is stable, values less than one are decreasing, and values greater than one are increasing. Species with the highest population growth rates are highlighted. Panel (b) shows the locations of breeding bird survey range centroids in 1997 and 2018 for each highlighted species, along with blue points that represent survey routes where the species was estimated to be present in at least one year.

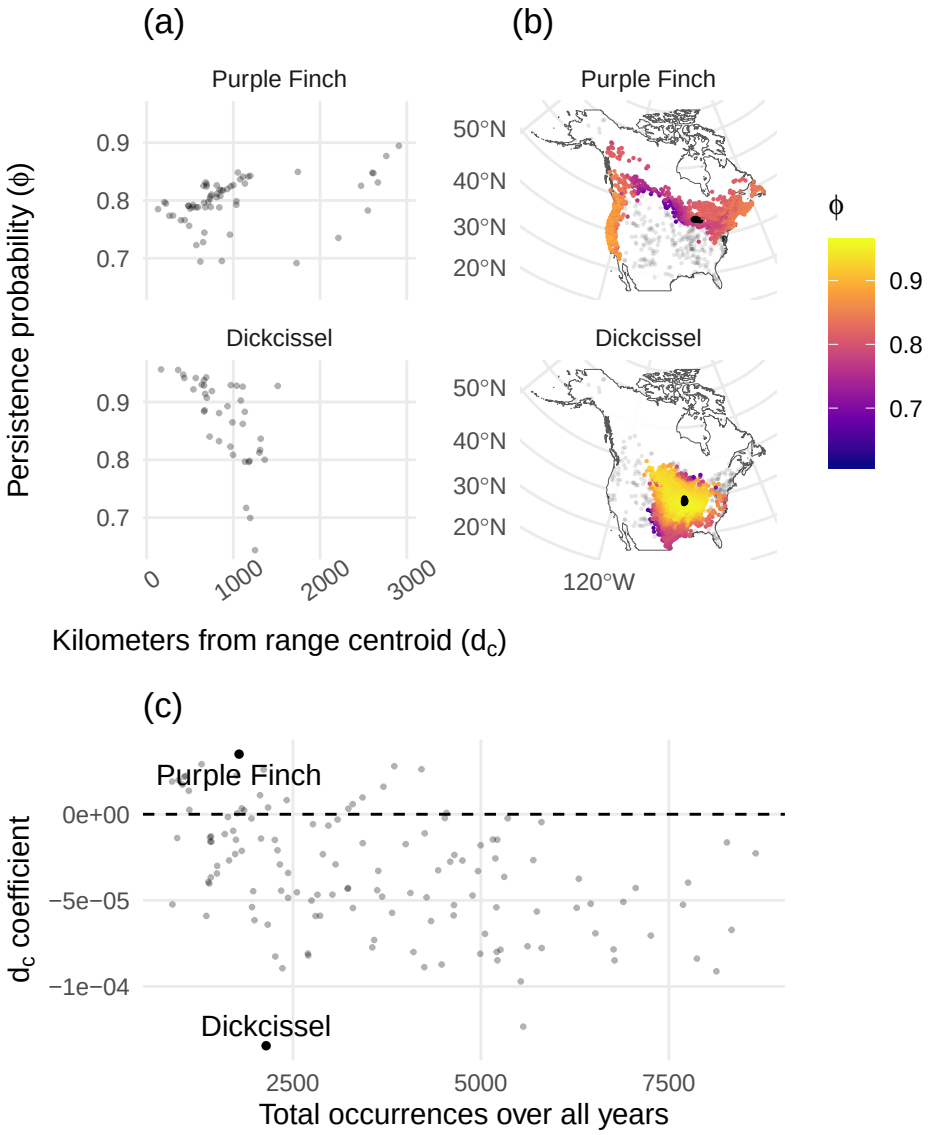

Figure 4: (a) Persistence probabilities (y-axis) as a function of distance from range centroid, averaged across years for the species with the largest positive relationship between distance from range centroid and persistence probability (top row), and largest negative relationship (bottom row). Each point represents a North American Breeding Bird Survey route. (b) Maps of persistence probabilities at each breeding bird survey route where these species were estimated to be present (in color), with route locations where the species was never estimated to be present in grey. Centroids for each year are shown in solid black. (c) Scatter plot relating the total number of occurrences across all routes and years (x-axis) to the slope of the relationship between distance from range centroid and persistence probability (d_c, on the y-axis). Each point represents a species. Points below the dashed line correspond to species with lower persistence at routes distant from their range centroids.

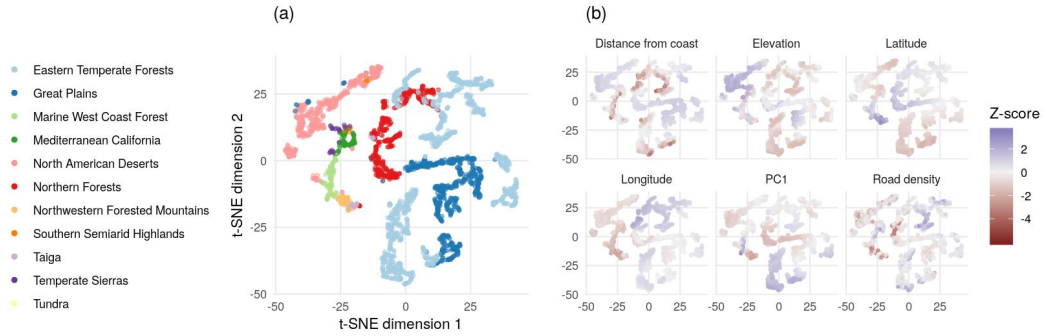

Figure 5: A two dimensional plot of North American Breeding Bird Survey route embeddings, computed using t-distributed stochastic neighbor embedding (t-SNE) on the latent vectors for initial occupancy, persistence, colonization, and detection probabilities for each route. Color indicates (a) EPA level 1 ecoregion and (b) z-standardized continuous route-level features. PC1 refers to the first principal component of WorldClim climate data. Notice clustering both by ecoregion, and by continuous route-level features.

The majority (82%) of common species were less likely to persist at routes that were distant from their estimated BBS range centroids. Examples from the species with the greatest positive and negative relationships between centroid distance and persistence are shown in Fig. 4a-b. Species that occurred in many routes and in many years tended to show consistently negative relationships between persistence and distance from range centroids (Fig. 4c).

Route vectors combined information from the categorical and continuous route-level features. Unsurprisingly (because ecoregion was an input feature), routes in the same ecoregions clustered together (Fig. 5a). Route embeddings also capture learned relationships among ecoregions. For example, Marine West Coast Forest ecoregion routes were similar to Northwestern Forested Mountains routes, and most different from Eastern Temperate Forests routes (Fig. 5a). Variation within clusters also related to continuous route-level features (Fig. 5b).

The model predicted non-linear dependence among species that is interpretable in terms of the cosine similarity among species-specific weight vectors. For example, weights for Mourning Dove (*Zenaida macroura*) were closest to those of Brown-headed Cowbird (*Molothrus ater*), and most different from Wilson's Warbler (*Cardellina pusilla*) (Fig. 6a). On BBS routes where Mourning Doves are likely to occur, Brown-headed Cowbird are also likely to occur, and Wilson's Warbler are unlikely to occur. Species pairs of the most similar and most dissimilar loadings are also provided for Eurasian Collared-Dove and Wilson's Warbler (Fig. 6b-c).

Discussion

Neural hierarchical models provide a bridge between hierarchical models that make use of scientific knowledge, and neural networks that approximate functions over structured domains. This framework integrates multiple threads of research in science-based deep learning and ecological modeling, and can use existing hierarchical models as a starting point. The case study provides a proof of concept example of constructing a scalable and performant neural hierarchical model based on a multispecies dynamic occupancy model, providing insights about colonization and extinction dynamics of North American bird assemblages at a continental scale.

The analysis of breeding bird survey data indicate that neural hierarchical models can outperform simpler models. Notably, the final model was performant both quantitatively and qualitatively, detecting population increases and range expansions that are consistent with prior work. The case study extends previous analyses of persistence probabilities at range edges (Royle & Kéry 2007), indicating that common species tended to be more persistent at routes close to their BBS range centroid. The strongest exception to this trend might be a consequence of the centroid providing a poor measure of central tendency of the BBS range. In particular, for the Purple Finch (*Haemorhous purpureus*), which had the strongest positive relationship between persistence probability and distance from BBS range centroid, the BBS range is irregularly shaped such that the centroid lies at the range

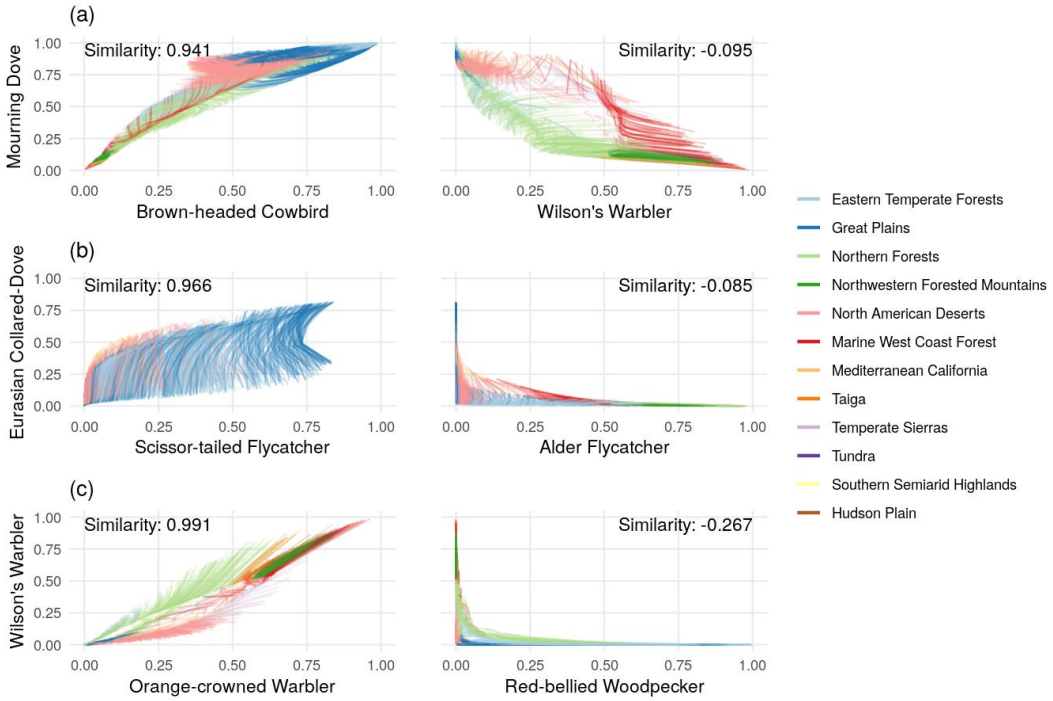

Figure 6: Relationships among species estimated occupancy probabilities through time, by location for species pairs that are nearest neighbors in weight cosine distance (left column), and most cosine dissimilar (right column). Color indicates EPA level 1 ecoregions. Cosine similarity values for species pairs are printed in the upper corners of each panel. Each route is a line segment that connects estimates of occupancy probabilities for each year from 1997 to 2018.

boundary, and the northern range of the species is not as well represented in BBS routes. This highlights some challenges posed by irregular range geometry and incomplete sampling of species ranges for macroecological studies that have been pointed out for similar questions about species abundance at observed range edges (Sagarin & Gaines 2002; Dallas *et al.* 2017; Knouft 2018).

The case study used a gated recurrent neural network architecture to capitalize on temporal structure (Chung *et al.* 2014), and architectures designed for other data structures present other opportunities for ecological applications. For example, neural hierarchical models could be used to couple a convolutional neural network observation model for camera trap images (Norouzzadeh *et al.* 2018; Tabak *et al.* 2019) with an ecological process model that describes animal density, movement, or community composition (Burton *et al.* 2015). Other ecological data structured on regular grids such as modeled climate data, remotely sensed Earth observations, and even 96 well microplates also might use convolutional neural network architectures. In addition, many ecological datasets exhibit graph structure related to phylogenies, social networks, or network-like spatial structure. While it is possible to adapt convolutional neural networks to operate on distance matrices computed from graphs (Fioravanti *et al.* 2018), there are a variety of graph representation learning approaches that provide embeddings for nodes that encode network structure and node attributes (Hamilton *et al.* 2017; Cai *et al.* 2018).

Neural hierarchical models can scale to data that are too large to fit in computer memory. This is particularly relevant for extensions of the BBS case study, given the volume of (imperfect) bird data accumulating through citizen science programs (Sullivan *et al.* 2009). The key strategy providing this scalability is stochastic optimization that uses mini-batches - small subsets of a larger dataset - that provide a noisy estimate of model performance and partial derivatives that can be used during training without ever needing to load the entire dataset into memory (Ruder 2016). This could be useful as a way to scale models that integrate BBS, eBird, and other data (Ngiam *et al.* 2011; Pacifici *et al.* 2017; Zipkin *et al.* 2017; Lin *et al.* n.d.).

Looking ahead, in a forecasting or decision-making setting, it would be important to estimate both aleatoric uncertainty (arising from noise in an observation process) and epistemic uncertainty (arising from uncertainty in a model and its parameters) (Clark *et al.* 2001; Kendall & Gal 2017). Recent advances in accounting for uncertainty in neural network parameter estimates and architectures could be applied in future work. Approaches include "Bayes by backpropagation" (Blundell *et al.* 2015), normalizing flows for variational approximations (Kingma *et al.* 2016), adversarial training (Lakshminarayanan *et al.* 2017), methods that use dropout or its continuous relaxation (Gal *et al.* 2017), and ensemble approaches (McDermott & Wikle 2017). In a decision-making context, interpretability and explainability also stands out as a key topic (Rudin 2018).

Neural networks have a reputation for being "black-box" models, but recent work provides tools that facilitate the interpretation and explanation of such models (Roscher *et al.* 2019). Interpretations map abstract concepts to domains that humans can make sense of, e.g., mapping latent vectors or weights of neural network to species identity or spatial location (Montavon *et al.* 2018). Explanations are collections of features in such a domain that contributed to a prediction (Montavon *et al.* 2018), e.g., sensitivity of model output to perturbations of the input (Olden & Jackson 2002; Gevrey *et al.* 2003).

The potential for combining neural networks with mechanistic models was recognized more than thirty years ago (Psichogios & Ungar 1992; Meade Jr & Fernandez 1994; Lagaris *et al.* 1998). This potential is more easily realized today due to methodological spillover from deep learning into the natural sciences, but also increases in computing power, availability of ecological data, and the proliferation of educational content for quantitative ecology and machine learning. Further, modern deep learning frameworks provide abstractions that allow users to focus on model construction rather than the details of implementation, increasing accessibility in the same way that WinBUGS, JAGS, OpenBUGS, and Stan have done (Lunn *et al.* 2000; Plummer & others 2003; Spiegelhalter *et al.* 2005; Carpenter *et al.* 2017).

Although deep learning and ecological modeling may seem to be separate activities, neural hierarchical models bridge these disciplines. Given the increasing availability of massive ecological data, scalable and flexible science-based models are increasingly needed. Neural hierarchical models satisfy this need, and can provide a framework that links imperfect observational data to ecological processes and mechanisms by construction.

Acknowledgements

Thanks to David Zonana and Roland Knapp for discussions on the potential of neural hierarchical models, and to Susie Ellis for providing feedback on a draft of the manuscript. Also thanks to Brandon Edwards for developing the bbsBayes R package, which was used to acquire and parse the North American Breeding Bird Survey data. This work was motivated by a workshop on machine learning in Earth science, hosted by Earth Lab and organized by the Federation of Earth Science Information Partners and the National Aeronatics and Space Administration Advanced Information Systems Technology program. This work was made possible by the CU Boulder Grand Challenge initiative and the Cooperative Institute for Research in the Environmental Sciences through their investment in Earth Lab. Thanks also to the thousands of U.S. and Canadian participants who annually perform and coordinate the North American Breeding Bird Survey.

Literature cited

Austin, M. (2002). Spatial prediction of species distribution: An interface between ecological theory and statistical modelling. *Ecological modelling*, 157, 101–118.

Berliner, L.M. (1996). Hierarchical bayesian time series models. In: *Maximum entropy and bayesian methods*. Springer, pp. 15–22.

Bingham, E., Chen, J.P., Jankowiak, M., Obermeyer, F., Pradhan, N. & Karaletsos, T. *et al.* (2018). Pyro: Deep Universal Probabilistic Programming. *arXiv preprint arXiv:1810.09538*.

Bled, F., Nichols, J.D. & Altwegg, R. (2013). Dynamic occupancy models for analyzing species' range dynamics across large geographic scales. *Ecology and evolution*, 3, 4896–4909.

Bled, F., Royle, J.A. & Cam, E. (2011). Hierarchical modeling of an invasive spread: The eurasian collared-dove streptopelia decaocto in the united states. *Ecological Applications*, 21, 290–302.

Blundell, C., Cornebise, J., Kavukcuoglu, K. & Wierstra, D. (2015). Weight uncertainty in neural networks. *arXiv preprint arXiv:1505.05424*.

Burton, A.C., Neilson, E., Moreira, D., Ladle, A., Steenweg, R. & Fisher, J.T. *et al.* (2015). Wildlife camera trapping: A review and recommendations for linking surveys to ecological processes. *Journal of Applied Ecology*, 52, 675–685.

Butler, K.T., Davies, D.W., Cartwright, H., Isayev, O. & Walsh, A. (2018). Machine learning for molecular and materials science. *Nature*, 559, 547.

Cai, H., Zheng, V.W. & Chang, K.C.-C. (2018). A comprehensive survey of graph embedding: Problems, techniques, and applications. *IEEE Transactions on Knowledge and Data Engineering*, 30, 1616–1637.

Calvert, A.M., Bonner, S.J., Jonsen, I.D., Flemming, J.M., Walde, S.J. & Taylor, P.D. (2009). A hierarchical bayesian approach to multi-state mark–recapture: Simulations and applications. *Journal of Applied Ecology*, 46, 610–620.

Carleo, G., Cirac, I., Cranmer, K., Daudet, L., Schuld, M. & Tishby, N. *et al.* (2019). Machine learning and the physical sciences. *arXiv preprint arXiv:1903.10563*.

Carpenter, B., Gelman, A., Hoffman, M.D., Lee, D., Goodrich, B. & Betancourt, M. *et al.* (2017). Stan: A probabilistic programming language. *Journal of statistical software*, 76.

Chen, D.-G. & Hare, S.R. (2006). Neural network and fuzzy logic models for pacific halibut recruitment analysis. *ecological modelling*, 195, 11–19.

Chen, D., Xue, Y., Chen, S., Fink, D. & Gomes, C. (2016). Deep multi-species embedding. *arXiv preprint arXiv:1609.09353*.

Ching, T., Himmelstein, D.S., Beaulieu-Jones, B.K., Kalinin, A.A., Do, B.T. & Way, G.P. *et al.* (2018). Opportunities and obstacles for deep learning in biology and medicine. *Journal of The Royal Society Interface*, 15, 20170387.

Chon, T.-S., Kwak, I.-S., Park, Y.-S., Kim, T.-H. & Kim, Y. (2001). Patterning and short-term predictions of benthic macroinvertebrate community dynamics by using a recurrent artificial neural network. *Ecological Modelling*, 146, 181–193.

Christin, S., Hervet, E. & Lecomte, N. (2018). Applications for deep learning in ecology. *bioRxiv*, 334854.

Chung, J., Gulcehre, C., Cho, K. & Bengio, Y. (2014). Empirical evaluation of gated recurrent neural networks on sequence modeling. *arXiv preprint arXiv:1412.3555*.

Clark, J.S., Carpenter, S.R., Barber, M., Collins, S., Dobson, A. & Foley, J.A. *et al.* (2001). Ecological forecasts: An emerging imperative. *science*, 293, 657–660.

Cressie, N., Calder, C.A., Clark, J.S., Hoef, J.M.V. & Wikle, C.K. (2009). Accounting for uncertainty in ecological analysis: The strengths and limitations of hierarchical statistical modeling. *Ecological Applications*, 19, 553–570.

Cybenko, G. (1989). Approximation by superpositions of a sigmoidal function. *Mathematics of control, signals and systems*, 2, 303–314.

Dallas, T., Decker, R.R. & Hastings, A. (2017). Species are not most abundant in the centre of their geographic range or climatic niche. *Ecology Letters*, 20, 1526–1533.

Dennis, E.B., Morgan, B.J. & Ridout, M.S. (2015). Computational aspects of n-mixture models. *Biometrics*, 71, 237–246.

Desjardins-Proulx, P., Poisot, T. & Gravel, D. (2019). Artificial intelligence for ecological and evolutionary synthesis. *bioRxiv*.

De Valpine, P. & Hastings, A. (2002). Fitting population models incorporating process noise and observation error. *Ecological Monographs*, 72, 57–76.

Dorazio, R.M., Kery, M., Royle, J.A. & Plattner, M. (2010). Models for inference in dynamic metacommunity systems. *Ecology*, 91, 2466–2475.

Fick, S.E. & Hijmans, R.J. (2017). WorldClim 2: New 1-km spatial resolution climate surfaces for global land areas. *International journal of climatology*, 37, 4302–4315.

Fioravanti, D., Giarratano, Y., Maggio, V., Agostinelli, C., Chierici, M. & Jurman, G. *et al.* (2018). Phylogenetic convolutional neural networks in metagenomics. *BMC bioinformatics*, 19, 49.

Flagel, L., Brandvain, Y. & Schrider, D.R. (2018). The unreasonable effectiveness of convolutional neural networks in population genetic inference. *Molecular biology and evolution*, 36, 220–238.

Gal, Y., Hron, J. & Kendall, A. (2017). Concrete dropout. In: *Advances in neural information processing systems*. pp. 3581–3590.

Gazestani, V.H. & Lewis, N.E. (2019). From genotype to phenotype: Augmenting deep learning with networks and systems biology. *Current Opinion in Systems Biology*.

Gevrey, M., Dimopoulos, I. & Lek, S. (2003). Review and comparison of methods to study the contribution of variables in artificial neural network models. *Ecological modelling*, 160, 249–264.

Golding, N. & Purse, B.V. (2016). Fast and flexible bayesian species distribution modelling using gaussian processes. *Methods in Ecology and Evolution*, 7, 598–608.

Goodfellow, I., Bengio, Y. & Courville, A. (2016). *Deep learning*. MIT press.

Guillera-Arroita, G. (2017). Modelling of species distributions, range dynamics and communities under imperfect detection: Advances, challenges and opportunities. *Ecography*, 40, 281–295.

Guo, C. & Berkhahn, F. (2016). Entity embeddings of categorical variables. *arXiv preprint arXiv:1604.06737*.

Hamilton, W., Ying, Z. & Leskovec, J. (2017). Inductive representation learning on large graphs. In: *Advances in neural information processing systems*. pp. 1024–1034.

Harris, D.J. (2015). Generating realistic assemblages with a joint species distribution model. *Methods in Ecology and Evolution*, 6, 465–473.

Hefley, T.J., Broms, K.M., Brost, B.M., Buderman, F.E., Kay, S.L. & Scharf, H.R. *et al.* (2017). The basis function approach for modeling autocorrelation in ecological data. *Ecology*, 98, 632–646.

Hochreiter, S. & Schmidhuber, J. (1997). Long short-term memory. *Neural computation*, 9, 1735–1780.

Hornik, K. (1991). Approximation capabilities of multilayer feedforward networks. *Neural networks*, 4, 251–257.

Hutchinson, R.A., Liu, L.-P. & Dietterich, T.G. (2011). Incorporating boosted regression trees into ecological latent variable models. In: *Twenty-fifth aaai conference on artificial intelligence*.

Jain, A., Zamir, A.R., Savarese, S. & Saxena, A. (2016). Structural-rnn: Deep learning on spatio-temporal graphs. In: *Proceedings of the ieee conference on computer vision and pattern recognition*. pp. 5308–5317.

Jeong, K.-S., Joo, G.-J., Kim, H.-W., Ha, K. & Recknagel, F. (2001). Prediction and elucidation of phytoplankton dynamics in the nakdong river (korea) by means of a recurrent artificial neural network. *Ecological Modelling*, 146, 115–129.

Jeong, K.-S., Kim, D.-K., Jung, J.-M., Kim, M.-C. & Joo, G.-J. (2008). Non-linear autoregressive modelling by temporal recurrent neural networks for the prediction of freshwater phytoplankton dynamics. *ecological modelling*, 211, 292–300.

Johnson, D.S., Laake, J.L. & Ver Hoef, J.M. (2010). A model-based approach for making ecological inference from distance sampling data. *Biometrics*, 66, 310–318.

Johnson, D.S., Thomas, D.L., Ver Hoef, J.M. & Christ, A. (2008). A general framework for the analysis of animal resource selection from telemetry data. *Biometrics*, 64, 968–976.

Jolly, G.M. (1965). Explicit estimates from capture-recapture data with both death and immigration-stochastic model. *Biometrika*, 52, 225–247.

Karpatne, A., Watkins, W., Read, J. & Kumar, V. (2017). Physics-guided neural networks (pgnn): An application in lake temperature modeling. *arXiv preprint arXiv:1710.11431*.

Kendall, A. & Gal, Y. (2017). What uncertainties do we need in bayesian deep learning for computer vision? In: *Advances in neural information processing systems*. pp. 5574–5584.

King, R. (2012). A review of bayesian state-space modelling of capture–recapture–recovery data. *Interface Focus*, 2, 190–204.

Kingma, D.P., Salimans, T., Jozefowicz, R., Chen, X., Sutskever, I. & Welling, M. (2016). Improved variational inference with inverse autoregressive flow. In: *Advances in neural information processing systems*. pp. 4743–4751.

Knapp, R.A., Matthews, K.R., Preisler, H.K. & Jellison, R. (2003). Developing probabilistic models to predict amphibian site occupancy in a patchy landscape. *Ecological Applications*, 13, 1069–1082.

Knouft, J.H. (2018). Appropriate application of information from biodiversity databases is critical when investigating species distributions and diversity: A comment on dallas et al.(). *Ecology letters*, 21, 1119–1120.

Krishnan, R.G., Shalit, U. & Sontag, D. (2017). Structured inference networks for nonlinear state space models. In: *Thirty-first aaai conference on artificial intelligence*.

Lagaris, I.E., Likas, A. & Fotiadis, D.I. (1998). Artificial neural networks for solving ordinary and partial differential equations. *IEEE transactions on neural networks*, 9, 987–1000.

Lakshminarayanan, B., Pritzel, A. & Blundell, C. (2017). Simple and scalable predictive uncertainty estimation using deep ensembles. In: *Advances in neural information processing systems*. pp. 6402–6413.

Langrock, R., King, R., Matthiopoulos, J., Thomas, L., Fortin, D. & Morales, J.M. (2012). Flexible and practical modeling of animal telemetry data: Hidden markov models and extensions. *Ecology*, 93, 2336–2342.

Latimer, A., Banerjee, S., Sang Jr, H., Mosher, E. & Silander Jr, J. (2009). Hierarchical models facilitate spatial analysis of large data sets: A case study on invasive plant species in the northeastern united states. *Ecology Letters*, 12, 144–154.

LeCun, Y., Bengio, Y. & Hinton, G. (2015). Deep learning. *nature*, 521, 436.

Lek, S., Delacoste, M., Baran, P., Dimopoulos, I., Lauga, J. & Aulagnier, S. (1996). Application of neural networks to modelling nonlinear relationships in ecology. *Ecological modelling*, 90, 39–52.

Li, Y., Bu, R., Sun, M., Wu, W., Di, X. & Chen, B. (2018). PointCNN: Convolution on x-transformed points. In: *Advances in neural information processing systems*. pp. 820–830.

Lin, T.-Y., Winner, K., Bernstein, G., Mittal, A., Dokter, A.M. & Horton, K.G. *et al.* (n.d.). MistNet: Measuring historical bird migration in the us using archived weather radar data and convolutional neural networks. *Methods in Ecology and Evolution*, In press.

Link, W.A. & Sauer, J.R. (1998). Estimating population change from count data: Application to the north american breeding bird survey. *Ecological applications*, 8, 258–268.

Long, J., Shelhamer, E. & Darrell, T. (2015). Fully convolutional networks for semantic segmentation. In: *Proceedings of the ieee conference on computer vision and pattern recognition*. pp. 3431–3440.

Lu, Z., Pu, H., Wang, F., Hu, Z. & Wang, L. (2017). The expressive power of neural networks: A view from the width. In: *Advances in neural information processing systems*. pp. 6231–6239.

Lunn, D.J., Thomas, A., Best, N. & Spiegelhalter, D. (2000). WinBUGS-a bayesian modelling framework: Concepts, structure, and extensibility. *Statistics and computing*, 10, 325–337.

Maaten, L. van der & Hinton, G. (2008). Visualizing data using t-sne. *Journal of machine learning research*, 9, 2579–2605.

MacKenzie, D.I., Nichols, J.D., Hines, J.E., Knutson, M.G. & Franklin, A.B. (2003). Estimating site occupancy, colonization, and local extinction when a species is detected imperfectly. *Ecology*, 84, 2200–2207.

MacKenzie, D.I., Nichols, J.D., Lachman, G.B., Droege, S., Andrew Royle, J. & Langtimm, C.A. (2002). Estimating site occupancy rates when detection probabilities are less than one. *Ecology*, 83, 2248–2255.

Malek, S., Salleh, A., Milow, P., Baba, M.S. & Sharifah, S. (2012). Applying artificial neural network theory to exploring diatom abundance at tropical putrajaya lake, malaysia. *Journal of freshwater ecology*, 27, 211–227.

Manel, S., Dias, J.-M. & Ormerod, S.J. (1999). Comparing discriminant analysis, neural networks and logistic regression for predicting species distributions: A case study with a himalayan river bird. *Ecological modelling*, 120, 337–347.

McDermott, P.L. & Wikle, C.K. (2017). An ensemble quadratic echo state network for non-linear spatio-temporal forecasting. *Stat*, 6, 315–330.

McDermott, P.L. & Wikle, C.K. (2019). Deep echo state networks with uncertainty quantification for spatio-temporal forecasting. *Environmetrics*, 30, e2553.

Meade Jr, A.J. & Fernandez, A.A. (1994). The numerical solution of linear ordinary differential equations by feedforward neural networks. *Mathematical and Computer Modelling*, 19, 1–25.

Mehlman, D.W. (1997). Change in avian abundance across the geographic range in response to environmental change. *Ecological Applications*, 7, 614–624.

Meijer, J.R., Huijbregts, M.A., Schotten, K.C. & Schipper, A.M. (2018). Global patterns of current and future road infrastructure. *Environmental Research Letters*, 13, 064006.

Miller, D.L., Burt, M.L., Rexstad, E.A. & Thomas, L. (2013). Spatial models for distance sampling data: Recent developments and future directions. *Methods in Ecology and Evolution*, 4, 1001–1010.

Montavon, G., Samek, W. & Müller, K.-R. (2018). Methods for interpreting and understanding deep neural networks. *Digital Signal Processing*, 73, 1–15.

Nair, V. & Hinton, G.E. (2010). Rectified linear units improve restricted boltzmann machines. In: *Proceedings of the 27th international conference on machine learning (icml-10)*. pp. 807–814.

Ngiam, J., Khosla, A., Kim, M., Nam, J., Lee, H. & Ng, A.Y. (2011). Multimodal deep learning. In: *Proceedings of the 28th international conference on machine learning (icml-11)*. pp. 689–696.

Niepert, M., Ahmed, M. & Kutzkov, K. (2016). Learning convolutional neural networks for graphs. In: *International conference on machine learning*. pp. 2014–2023.

Norouzzadeh, M.S., Nguyen, A., Kosmala, M., Swanson, A., Palmer, M.S. & Packer, C. *et al.* (2018). Automatically identifying, counting, and describing wild animals in camera-trap images with deep learning. *Proceedings of the National Academy of Sciences*, 115, E5716–E5725.

Oksanen, J. & Minchin, P.R. (2002). Continuum theory revisited: What shape are species responses along ecological gradients? *Ecological Modelling*, 157, 119–129.

Olden, J.D. & Jackson, D.A. (2002). Illuminating the "black box": A randomization approach for understanding variable contributions in artificial neural networks. *Ecological modelling*, 154, 135–150.

Ovaskainen, O., Roy, D.B., Fox, R. & Anderson, B.J. (2016). Uncovering hidden spatial structure in species communities with spatially explicit joint species distribution models. *Methods in Ecology and Evolution*, 7, 428–436.

Özesmi, S.L., Tan, C.O. & Özesmi, U. (2006). Methodological issues in building, training, and testing artificial neural networks in ecological applications. *Ecological Modelling*, 195, 83–93.

Pacifici, K., Reich, B.J., Miller, D.A., Gardner, B., Stauffer, G. & Singh, S. *et al.* (2017). Integrating multiple data sources in species distribution modeling: A framework for data fusion. *Ecology*, 98, 840–850.

Paganini, M., Oliveira, L. de & Nachman, B. (2018). Accelerating science with generative adversarial networks: An application to 3D particle showers in multilayer calorimeters. *Physical review letters*, 120, 042003.

Pardieck, L., K., Ziolkowski Jr., J., D., M., L. & Aponte *et al.* (2018). North american breeding bird survey dataset 1966 - 2018.

Paszke, A., Gross, S., Chintala, S., Chanan, G., Yang, E. & DeVito, Z. *et al.* (2017). Automatic differentiation in PyTorch. In: *NIPS autodiff workshop*.

Patterson, T.A., Basson, M., Bravington, M.V. & Gunn, J.S. (2009). Classifying movement behaviour in relation to environmental conditions using hidden markov models. *Journal of Animal Ecology*, 78, 1113–1123.

Plummer, M. & others. (2003). JAGS: A program for analysis of bayesian graphical models using gibbs sampling. In: *Proceedings of the 3rd international workshop on distributed statistical computing*. Vienna, Austria.

Psichogios, D.C. & Ungar, L.H. (1992). A hybrid neural network-first principles approach to process modeling. *AIChE Journal*, 38, 1499–1511.

Rabiner, L.R. (1989). A tutorial on hidden markov models and selected applications in speech recognition. *Proceedings of the IEEE*, 77, 257–286.

Radovic, A., Williams, M., Rousseau, D., Kagan, M., Bonacorsi, D. & Himmel, A. *et al.* (2018). Machine learning at the energy and intensity frontiers of particle physics. *Nature*, 560, 41.

Raissi, M. (2018). Deep hidden physics models: Deep learning of nonlinear partial differential equations. *The Journal of Machine Learning Research*, 19, 932–955.

Rangapuram, S.S., Seeger, M.W., Gasthaus, J., Stella, L., Wang, Y. & Januschowski, T. (2018). Deep state space models for time series forecasting. In: *Advances in neural information processing systems*. pp. 7785–7794.

Rauber, P.E., Fadel, S.G., Falcao, A.X. & Telea, A.C. (2016). Visualizing the hidden activity of artificial neural networks. *IEEE transactions on visualization and computer graphics*, 23, 101–110.

Reichstein, M., Camps-Valls, G., Stevens, B., Jung, M., Denzler, J. & Carvalhais, N. *et al.* (2019). Deep learning and process understanding for data-driven earth system science. *Nature*, 566, 195.

Roberts, D.R., Bahn, V., Ciuti, S., Boyce, M.S., Elith, J. & Guillera-Arroita, G. *et al.* (2017). Cross-validation strategies for data with temporal, spatial, hierarchical, or phylogenetic structure. *Ecography*, 40, 913–929.

Roscher, R., Bohn, B., Duarte, M.F. & Garcke, J. (2019). Explainable machine learning for scientific insights and discoveries. *arXiv preprint arXiv:1905.08883*.

Royle, J.A. (2004). N-mixture models for estimating population size from spatially replicated counts. *Biometrics*, 60, 108–115.

Royle, J.A. & Kéry, M. (2007). A bayesian state-space formulation of dynamic occupancy models. *Ecology*, 88, 1813–1823.

Royle, J.A. & Link, W.A. (2006). Generalized site occupancy models allowing for false positive and false negative errors. *Ecology*, 87, 835–841.

Ruder, S. (2016). An overview of gradient descent optimization algorithms. *arXiv preprint arXiv:1609.04747*.

Rudin, C. (2018). Please stop explaining black box models for high stakes decisions. *arXiv preprint arXiv:1811.10154*.

Russell, S.J. & Norvig, P. (2016). *Artificial intelligence: A modern approach*. Malaysia; Pearson Education Limited,

Sagarin, R.D. & Gaines, S.D. (2002). The 'abundant centre'distribution: To what extent is it a biogeographical rule? *Ecology letters*, 5, 137–147.

Sauer, J.R. & Link, W.A. (2011). Analysis of the north american breeding bird survey using hierarchical models. *The Auk*, 128, 87–98.

Sauer, J.R., Link, W.A., Fallon, J.E., Pardieck, K.L. & Ziolkowski Jr, D.J. (2013). The north american breeding bird survey 1966–2011: Summary analysis and species accounts. *North American Fauna*, 79, 1–32.

Sauer, J.R., Niven, D.K., Pardieck, K.L., Ziolkowski Jr, D.J. & Link, W.A. (2017). Expanding the north american breeding bird survey analysis to include additional species and regions. *Journal of Fish and Wildlife Management*, 8, 154–172.

Spiegelhalter, D., Thomas, A., Best, N. & Lunn, D. (2005). OpenBUGS version 2.10, user manual. *MRC Biostatistics Unit, Cambridge, United Kingdom*.

Stan Development Team. (2018). RStan: The R interface to Stan.

Sullivan, B.L., Wood, C.L., Iliff, M.J., Bonney, R.E., Fink, D. & Kelling, S. (2009). EBird: A citizen-based bird observation network in the biological sciences. *Biological Conservation*, 142, 2282–2292.

Sutskever, I., Vinyals, O. & Le, Q.V. (2014). Sequence to sequence learning with neural networks. In: *Advances in neural information processing systems*. pp. 3104–3112.

Tabak, M.A., Norouzzadeh, M.S., Wolfson, D.W., Sweeney, S.J., VerCauteren, K.C. & Snow, N.P. *et al.* (2019). Machine learning to classify animal species in camera trap images: Applications in ecology. *Methods in Ecology and Evolution*, 10, 585–590.

Thorson, J.T., Ianelli, J.N., Larsen, E.A., Ries, L., Scheuerell, M.D. & Szuwalski, C. *et al.* (2016). Joint dynamic species distribution models: A tool for community ordination and spatio-temporal monitoring. *Global Ecology and Biogeography*, 25, 1144–1158.

Thorson, J.T., Scheuerell, M.D., Shelton, A.O., See, K.E., Skaug, H.J. & Kristensen, K. (2015). Spatial factor analysis: A new tool for estimating joint species distributions and correlations in species range. *Methods in Ecology and Evolution*, 6, 627–637.

Tikhonov, G., Abrego, N., Dunson, D. & Ovaskainen, O. (2017). Using joint species distribution models for evaluating how species-to-species associations depend on the environmental context. *Methods in Ecology and Evolution*, 8, 443–452.

Tobler, M.W., Kéry, M., Hui, F.K., Guillera-Arroita, G., Knaus, P. & Sattler, T. (2019). Joint species distribution models with species correlations and imperfect detection. *Ecology*, e02754.

Van Lint, J., Hoogendoorn, S. & Zuylen, H.J. van. (2002). Freeway travel time prediction with state-space neural networks: Modeling state-space dynamics with recurrent neural networks. *Transportation Research Record*, 1811, 30–39.

Viterbi, A. (1967). Error bounds for convolutional codes and an asymptotically optimum decoding algorithm. *IEEE transactions on Information Theory*, 13, 260–269.

Warton, D.I., Blanchet, F.G., O'Hara, R.B., Ovaskainen, O., Taskinen, S. & Walker, S.C. *et al.* (2015). So many variables: Joint modeling in community ecology. *Trends in Ecology & Evolution*, 30, 766–779.

Webb, M.H., Wotherspoon, S., Stojanovic, D., Heinsohn, R., Cunningham, R. & Bell, P. *et al.* (2014). Location matters: Using spatially explicit occupancy models to predict the distribution of the highly mobile, endangered swift parrot. *Biological Conservation*, 176, 99–108.

Wikle, C.K. (2003). Hierarchical models in environmental science. *International Statistical Review*, 71, 181–199.

Wikle, C.K. (2019). Comparison of deep neural networks and deep hierarchical models for spatio-temporal data. *Journal of Agricultural, Biological and Environmental Statistics*, 1–29.

Xingjian, S., Chen, Z., Wang, H., Yeung, D.-Y., Wong, W.-K. & Woo, W.-c. (2015). Convolutional lstm network: A machine learning approach for precipitation nowcasting. In: *Advances in neural information processing systems*. pp. 802–810.

Xu, B., Wang, N., Chen, T. & Li, M. (2015). Empirical evaluation of rectified activations in convolutional network. *arXiv preprint arXiv:1505.00853*.

Yuan, Y., Bachl, F.E., Lindgren, F., Borchers, D.L., Illian, J.B. & Buckland, S.T. *et al.* (2017). Point process models for spatio-temporal distance sampling data from a large-scale survey of blue whales. *The Annals of Applied Statistics*, 11, 2270–2297.

Zamarreño, J.M. & Vega, P. (1998). State space neural network. Properties and application. *Neural networks*, 11, 1099–1112.

Zipkin, E.F., Rossman, S., Yackulic, C.B., Wiens, J.D., Thorson, J.T. & Davis, R.J. *et al.* (2017). Integrating count and detection–nondetection data to model population dynamics. *Ecology*, 98, 1640–1650.

Zucchini, W., MacDonald, I.L. & Langrock, R. (2017). *Hidden markov models for time series: An introduction using r*. Chapman; Hall/CRC.

Zwane, E. & Van der Heijden, P. (2004). Semiparametric models for capture–recapture studies with covariates. *Computational Statistics & Data Analysis*, 47, 729–743.

Appendix S1

This appendix includes example specifications for neural occupancy, N-mixture, and hidden Markov models. The goal in providing these specifications is to give concrete examples of neural hierarchical models that are relatively simple, while drawing connections to existing models. Pytorch implementations in Jupyter notebooks are available at https://github.com/mbjoseph/neuralecology.

Generally, the construction of a hierarchical model requires:

1. A **process model** that represents some ecological dynamics or states that can depend on unknown parameters.
2. An **observation model** that relates available data to the process model, possibly dependent on unknown parameters.
3. A **parameter model** for unknown quantities (e.g., their dependence on some input, or relationship to each other). Traditionally, this is discussed in terms of prior distributions, though there may be rich structure encoded in a parameter model as well (Wikle 2003). For a fully Bayesian hierarchical model, all unknowns are represented by probability distributions. In an empirical Bayesian hierarchical model, point estimates are typically used for top-level parameters instead, so that these top-level parameters are treated as fixed, but unknown (Cressie *et al.* 2009). In the examples below, neural networks are applied at the parameter model stage to learn a mapping from inputs to parameters of process and observation models.

Given these components, parameter estimation can proceed in a few ways, depending on the inferential framework used. A loss function can be constructed to find the parameter values that maximize the probability of the data, possibly with some penalties for model complexity (in a maximum likelihood/penalized maximum likelihood framework), find the most probable parameter values, conditional on the data (in a maximum *a posteriori* framework), or compute a probability distribution for all unknowns, conditional on the data (in a Bayesian framework). For many models applied in deep learning, it is often the case that fully Bayesian inference is complicated by high-dimensional multimodal posterior geometry.

The examples here focus primarily on penalized maximum likelihood methods, though Bayesian approaches stand out as a key area for future work (see main text for relevant citations). Often, L_2 norm penalties (also referred to as "weight decay") are applied on the weights of neural networks in the loss function to penalize model complexity in an effort to avoid overfitting. Additional strategies include early stopping, where an iterative stochastic optimization scheme is terminated before the training set loss stabilizes (or when the validation set loss begins to increase), which is particularly useful for complex models that can overfit quickly. Finally, unlike maximum likelihood estimation for simple models, because of the multimodality of the likelihood surface for neural network weights, there are no guarantees that a global maximum exists, or that a particular optimum is not a local maximum. In practice, this is not a major limitation. For more discussion, see Goodfellow *et al.* (2016).

A single-species single-season neural occupancy model

A single-species single-season occupancy model estimates presence/absence states from imperfect detection/non-detection data (MacKenzie *et al.* 2002). Assume that n spatial locations are each surveyed k times, during a short time interval for which it is reasonable to assume that the presence or absence of a species is constant. Each spatial location has some continuous covariate value represented by x_i for site $i = 1, ..., n$, that relates to occupancy and detection probabilities.

Observation model

Observations at site i consist of k surveys, where each survey results in a detection or non-detection. Let y_i represent the number of surveys at site i for which a species is detected, and z_i represent the true presence/absence state (if the species is present: $z_i = 1$; if absent: $z_i = 0$). Assuming that the probability of detecting a species on a survey conditional on presence is p_i, and that each survey is conditionally independent, the observations can be modeled with a Binomial distribution:

$$y_i \sim \text{Binomial}(z_i p_i, k).$$

Process model

The true presence/absence occupancy state z can be treated as a Bernoulli random variable, with occupancy probability ψ_i:

$$z_i \sim \text{Bernoulli}(\psi_i).$$

Parameter model

A simple approach to account for the effect of the site-level covariate on occupancy and detection would be to include a slope and intercept parameter specific to each component, using the logit function to ensure that estimated probabilities are bounded between 0 and 1:

$$\psi_i = \text{logit}^{-1}\big(\alpha^{(\psi)} + \beta^{(\psi)} x_i\big),$$
$$p_i = \text{logit}^{-1}\big(\alpha^{(p)} + \beta^{(p)} x_i\big),$$

where α^j and β^j are intercept and slope parameters for component j.

In contrast, a neural hierarchical model might instead account for site-level variation by modeling occupancy and detection probabilities as outputs of a neural network:

$$\begin{bmatrix} \psi_i \\ p_i \end{bmatrix} = f(x_i),$$

where $f(x_i)$ is a neural network that takes a scalar as input (the site-level covariate x_i) and outputs a two dimensional vector containing occupancy and detection probabilities:

$$f(x_i) = \text{logit}^{-1}\big(W^{(2)} g(W^{(1)} x_i)\big),$$

where $W^{(1)}$ and $W^{(2)}$ are weight matrices for the first and second layer, g is a differentiable nonlinear activation function, e.g., the rectified linear unit activation function (Nair & Hinton 2010), and the inverse logit transform is applied element-wise to ensure that ψ_i and p_i lie between 0 and 1.

Loss function

The negative log observed data likelihood can be taken as the loss function (MacKenzie *et al.* 2002). Marginalizing over z and treating sites as conditionally independent yields:

$$L(\theta_f) = -\sum_{i=1}^{n} \log \Big(\psi_i \text{Binomial}(y_i \mid p_i, k) + I(y_i = 0)(1 - \psi_i)\Big),$$

where θ_f represents the parameters of the neural network f, and $I(y_i = 0)$ is an indicator function equal to one when $y_i = 0$ (zero otherwise).

The loss for any particular site can be computed efficiently using the log-sum-exp trick, which is particularly useful when the log of summands is available (i.e., $\log(\psi_i) + \log\binom{k}{y_i} + y_i \log(p_i) + \log(k - y_i) + \log(1 - p_i)$ and $\log(1 - \psi_i)$ are already computed), as is the case in both Stan and Pytorch, which provide the log probability from the Binomial distribution.

A single-species neural dynamic occupancy model

A single-species dynamic occupancy model can be used to estimate rates of colonization and extinction when detection is imperfect and sites are repeatedly sampled at multiple time points (MacKenzie *et al.* 2003). Assume that for T timesteps, n spatial locations are each surveyed k times, during a short time interval for which it is reasonable to assume that the presence or absence state is constant. Among timesteps, the true occupancy states of sites can change. Each spatial location has some continuous covariate value represented by x_i for site $i = 1, ..., n$, that relates to occupancy and detection probabilities.

Observation model

Observations at site i in timestep t consist of k surveys, where each survey results in a detection or non-detection. Let $y_{i,t}$ represent the number of surveys at site i in timestep t for which a species is detected, and $z_{i,t}$ represent the true presence/absence state (if the species is present: $z_{i,t} = 1$; if absent: $z_{i,t} = 0$). Assuming that the probability of detecting a species on a survey conditional on presence is p_i, the observations can be modeled using a Binomial distribution:

$$y_{i,t} \sim \text{Binomial}(z_{i,t}p_i, k).$$

Process model

Sites can transition from being unoccupied ($z_{i,t} = 0$) to occupied ($z_{i,t+1} = 1$) due to colonization, or from being occupied ($z_{i,t} = 1$) to unoccupied ($z_{i,t+1} = 0$) due to extinction. Let the initial occupancy state be treated as a random Bernoulli variable with probability of occupancy $\psi_{i,1}$:

$$z_{i,1} \sim \text{Bernoulli}(\psi_{i,1}).$$

Subsequent occupancy dynamics at site i for timesteps $t = 1, ..., T$ are related to the probability of colonization (γ_i) and the probability of persistence (ϕ_i), where the extinction probability is taken to be the complement of persistence ($1 - \phi_i$).

$$z_{i,t} \sim \text{Bernoulli}(z_{i,t-1}\phi_i + (1 - z_{i,t-1})\gamma_i).$$

Parameter model

In this example, heterogeneity among sites was accounted for using a single layer neural network that ingests the one dimensional covariate x_i for site i, passes it through a single hidden layer, and outputs a four dimensional vector of probabilities containing the probabilities of initial occupancy ($\psi_{i,1}$), persistence (ϕ_i), colonization (γ_i), and detection (p_i):

$$\begin{bmatrix} \psi_{i,1} \\ \phi_i \\ \gamma_i \\ p_i \end{bmatrix} = f(x_i),$$

where f is a neural network. Concretely, f was parameterized as follows:

$$f(x_i) = \text{logit}^{-1}\Big(W^{(2)}g(W^{(1)}x_i)\Big),$$

where $W^{(1)}$ is a weight matrix that generates activations from the inputs, g is the ReLU activation function, $W^{(2)}$ is a weight matrix that maps the hidden layer to the outputs, and logit^{-1} is the element-wise inverse logistic (sigmoid) function.

Loss function

The negative log observed data likelihood was used as the loss function, implemented in Pytorch following the description in MacKenzie *et al.* (2003) (equation 5-6), assuming that detection histories for site $i = 1, ..., n$ are conditionally independent and scaling the forward probabilities to avoid underflow as described in Rabiner (1989).

A neural N-mixture model

An N-mixture model can be used to estimate latent integer-valued abundance when unmarked populations are repeatedly surveyed and it is assumed that detection of individuals is imperfect (Royle 2004). Assume that J spatial locations are each surveyed K times, in a short time interval for which it is reasonable to assume that the number of individuals is constant within locations $j = 1, ..., J$. Each spatial location has some continuous covariate value represented by x_j, that relates to detection probabilities and expected abundance.

Observation model

Observations at site j in survey k yield counts of the number of unique individuals detected, denoted $y_{j,k}$ for all j and all k. Assuming that the detection of each individual is conditionally independent, and that each individual is detected with site-specific probability p_j, the observations can be modeled with a Binomial distribution where the number of trials is the true (latent) population abundance n_j:

$$y_{j,k} \sim \text{Binomial}(p_j, n_j).$$

Process model

The true population abundance n_j is treated as a Poisson random variable with expected value λ_j:

$$n_j \sim \text{Poisson}(\lambda_j).$$

Parameter model

Heterogeneity among sites was accounted for using a single layer neural network that ingests the one dimensional covariate x_i for site i, passes it through a single hidden layer, and outputs a two dimensional vector containing a detection probability p_i and the expected abundance λ_i:

$$\begin{bmatrix} \lambda_i \\ p_i \end{bmatrix} = f(x_i),$$

where f is a neural network with two dimensional output activations $h(x_i)$ computed via:

$$h(x_i) = W^{(2)} g(W^{(1)} x_i),$$

and final outputs computed using the log and logit link functions for expected abundance and detection probability:

$$f(x_i) = \begin{bmatrix} \exp(h_1(x_i)) \\ \text{logit}^{-1}(h_2(x_i)) \end{bmatrix}.$$

Here too $W^{(1)}$ is a weight matrix that generates activations from the inputs, g is the rectified linear unit activation function, and $W^{(2)}$ is a weight matrix that maps the hidden layer to the outputs. Additionally $h_1(x_i)$ is the first element of the output activation vector, and $h_2(x_i)$ the second element.

Loss function

The negative log likelihood was used as the loss function, enumerating over a large range of potential values of the true abundance (from $\min(y_{j\cdot})$ to $5 \times \max(y_{j\cdot})$, where $y_{j\cdot}$ is a vector of counts of length K) to approximate the underlying infinite mixture model implied by the Poisson model of abundance (Royle 2004). It is also worth noting that alternative specifications based on a multivariate Poisson model are possible (Dennis *et al.* 2015).

A neural hidden Markov model: capture-recapture-recovery

Consider a capture-recapture-recovery study aimed at estimating time-varying parameters (King 2012). Assume that individuals $i = 1, ..., N$ are initially captured, marked, and released on timestep $t = 0$.

The state of an individual i on time step t is denoted $z_{i,t}$. Individuals are either alive ($z_{i,t} = 0$), recently dead such that their bodies are discoverable (and marks identifiable) ($z_{i,t} = 1$), or long dead such that their bodies are not discoverable and/or marks are no longer identifiable ($z_{i,t} = 2$).

Observation model

Observations $y_{i,t}$ are made on time steps $t = 1, ..., T$, and if an individual is detected alive on timestep t, $y_{i,t} = 1$, and if an individual is detected as recently dead $y_{i,t} = 2$, otherwise if the individual is not detected $y_{i,t} = 0$.

Let Ω_t denote a time-varying emission matrix containing state-dependent observation probabilities:

$$\Omega_t = \begin{bmatrix} 1 - p_t & p_t & 0 \\ 1 - \lambda_t & 0 & \lambda_t \\ 1 & 0 & 0 \end{bmatrix},$$

where p_t is the probability of detecting an individual on timestep t, conditional on the individual being alive, and λ_t is the probability of recovering a recently dead individual on timestep t that has died since timestep $t - 1$. The rows of the emission matrix correspond to states (alive, recently dead, long dead), and the columns correspond to observations (not detected, detected alive, detected dead).

Process model

At time t, the transition probability matrix Γ_t contains the probability of transitioning from row j to column k:

$$\Gamma_t = \begin{bmatrix} \phi_t & 1 - \phi_t & 0 \\ 0 & 0 & 1 \\ 0 & 0 & 1 \end{bmatrix},$$

where survival probability is $\phi_t = P(z_{i,t+1} = 0 \mid z_{i,t} = 0)$, dead individuals stay dead, and the rows and columns of the transition matrix correspond to states (alive, recently dead, long dead).

Parameter Model

Heterogeneity among timesteps was accounted for using three two-layer neural networks (one for ϕ, one for λ, and one for p). Each network ingests a univariate time series and outputs a corresponding time series of parameter values (i.e., each network maps a sequence of inputs $x = (x_{t=1}, ..., x_{t=T})'$ to a sequence of parameter values, e.g., $p = (p_{t=1}, ..., p_{t=T})'$ for the detection probability network:

$$\begin{aligned} \phi &= \text{logit}^{-1} f^{(\phi)}(x), \\ \lambda &= \text{logit}^{-1} f^{(\lambda)}(x), \\ p &= \text{logit}^{-1} f^{(p)}(x), \end{aligned}$$

where f^j is a neural network for parameter j.

Loss function

The negative log observed data likelihood was used as the loss function, and computed using the forward algorithm (Zucchini *et al.* 2017). Observation histories for individuals were assumed to be conditionally independent. As an aside, one can specify such models in terms of the complete data likelihood (i.e., in terms of the hidden states) using programming frameworks that implement automatic enumeration of discrete latent variables with finite support, such as Pyro (Bingham *et al.* 2018).

Appendix S2

This appendix includes details on the structure and implementation of the baseline and neural dynamic occupancy models for breeding bird survey data.

Baseline model structure

The baseline model was a hierarchical Bayesian dynamic occupancy model, fit separately to each species. Let $s = 1, ..., S$ index survey routes, $t = 1, ..., T$ index years, and $j = 1, ..., J$ index bird species. Dropping subscripts for species j, for any particular species' model, presence/absence states are characterized by the following dynamics:

$$z_{t=1,s} \sim \text{Bernoulli}(\psi_{t=1,s}),$$

$$z_{t,s} \sim \text{Bernoulli}(\phi_s z_{t-1,s} + \gamma_s(1 - z_{t-1,s})), \quad \text{for } t = 2, ..., T,$$

where $\psi_{t,s}$ is the probability of occurrence at route s in year t, ϕ_s is the probability of persistence conditional on presence in the previous year, and γ_s is the probability of colonization conditional on absence in the previous year.

Detection/non-detection data arise via a binomial observation process:

$$y_{t,s} \sim \text{Binomial}(p_{t,s} z_{t,s}, 50),$$

for all s and t, where the binomial sample size 50 arises from having 50 stops along each route.

Heterogeneity in occupancy dynamics

Heterogeneity in occupancy dynamics was introduced in the model via additive adjustments for EPA level one ecoregions and route-level characteristics (centered and scaled to have mean zero and unit variance):

$$\text{logit}(\psi_{t=1,s}) = X_s \beta^{(\psi_1)} + \alpha^{(\psi_1)}_{r[s]},$$

where X_s is row s from the design matrix X containing the route-level features, $\beta^{(\psi_1)}$ is a parameter vector associated with initial occupancy, and EPA level one adjustments are denoted $\alpha^{(\psi_1)}_{r[s]}$, where $r[s]$ represents the region r containing route s. Similarly, persistence and colonization probabilities are modeled as:

$$\text{logit}(\phi_s) = X_s \beta^{(\phi)} + \alpha^{(\phi)}_{r[s]},$$

$$\text{logit}(\gamma_s) = X_s \beta^{(\gamma)} + \alpha^{(\gamma)}_{r[s]}.$$

Heterogeneity in observations

Heterogeneity in detection probability was included as:

$$\text{logit}(p_{t,s}) = X^{(p)}_{(s,t)} \beta^{(p)} + \alpha^{(p)}_{r[s]},$$

where $X^{(p)}_s$ is a augmented version of X_s that adds survey-level features related to detection probability (survey duration, along with start and end sky, temperature, and wind conditions, which vary by route and year), $\beta^{(p)}$ is a coefficient vector, and $\alpha^{(p)}_{r[s]}$ is an ecoregion adjustment.

Parameter model

Prior distributions were constructed to facilitate borrowing of information across the four parameter dimensions of initial occupancy, persistence, colonization, and detection. Ecoregion adjustments were assigned multivariate normal priors:

$$\begin{bmatrix} \alpha_r^{(\psi_1)} \\ \alpha_r^{(\phi)} \\ \alpha_r^{(\gamma)} \\ \alpha_r^{(p)} \end{bmatrix} \sim \text{MultivariateNormal}\big(0, \Sigma\big),$$

for regions $r = 1, ..., R$. The covariance matrix Σ was constructed for each level as $\Sigma = \text{diag}(\sigma)\Omega\text{diag}(\sigma)$, where σ is a vector of length 4, $\text{diag}(\sigma)$ is a 4×4 diagonal matrix with entries equal to σ, and Ω is a 4×4 correlation matrix.

Prior distributions were specified as follows:

$\sigma \sim \text{Gamma}(1.5, 10)$,
$\Omega \sim \text{LKJ-Correlation}(10)$,
$\beta^{(\psi_1)} \sim \text{Normal}(0, 1)$,
$\beta^{(\phi)} \sim \text{Normal}(0, 1)$,
$\beta^{(\gamma)} \sim \text{Normal}(0, 1)$,
$\beta^{(p)} \sim \text{Normal}(0, 1)$.

Posterior distribution

The posterior distribution is proportional to:

$$\prod_t \prod_s \text{Binomial}(y_{t,s} \mid z_{t,s} p_{t,s}, 50) \times$$
$$\prod_s \text{Bernoulli}(z_{t=1,s} \mid \psi_{t=1,s}) \prod_{t=2}^{T} \text{Bernoulli}(z_{t,s} \mid \phi_s z_{t-1,s} + \gamma_s(1 - z_{t-1,s})) \times$$
$$\prod_r [\alpha_r \mid \sigma, \Omega] \times$$
$$[\beta^{(\psi_1)}][\beta^{(\phi)}][\beta^{(\gamma)}][\beta^{(p)}][\sigma][\Omega].$$

Single species neural hierarchical model structure

The single species neural hierarchical model is a dynamic occupancy model parameterized by a neural network. Presence/absence states are characterized by the following dynamics:

$$z_{t=1,s} \sim \text{Bernoulli}(\psi_{t=1,s}),$$

$$z_{t,s} \sim \text{Bernoulli}(\phi_{t-1,s} z_{t-1,s} + \gamma_{t-1,s}(1 - z_{t-1,s})), \quad \text{for } t = 2, ..., T,$$

where $\psi_{t,s}$ is the probability of occurrence at route s in year t, $\phi_{t-1,s}$ is the probability of persistence conditional on presence in the previous year: $\Pr(z_{t,s} = 1 | z_{t-1,s} = 1) = \phi_{t-1,s}$, and $\gamma_{t-1,s}$ is the probability of colonization conditional on absence in the previous year: $\Pr(z_{t,s} = 1 | z_{t-1,s} = 0) = \gamma_{t-1,s}$.

Detection data are modeled using a binomial distribution:

$$y_{t,s} \sim \text{Binomial}(z_{t,s} p_{t,s}, 50),$$

for all s, and t.

Parameter model

Heterogeneity in occupancy and observation parameters was included by modeling initial occupancy, persistence, colonization, and detection probabilities as outputs of a neural network (Fig. S1). Categorical inputs to the network included EPA level one ecoregions, which were mapped to 8 dimensional numeric vector embeddings, $h_r^{(L_1)}$ for regions $r = 1, ..., R$ (Guo & Berkhahn 2016). Categorical entity embeddings are equivalent to using one layer of a neural network with 8 dimensional output, where the inputs are one-hot encoded ecoregion codes, but in practice using an embedding layer is more computationally efficient because it capitalizes on the sparsity of a one-hot encoding.

For example, let R represent the number of level 1 ecoregions containing BBS routes ($R = 14$). Let $x_{r[s]}^{(L_1)}$ represent a one-hot encoded vector of length R, where all entries are zero except for the index of the level 1 ecoregion containing route s (denoted $r[s]$), which is set equal to one. Then, let $W^{(L_1)}$ represent a weight matrix of size $D^{(L_1)} \times R$, where $D^{(L_1)}$ is the dimensionality of the embedding ($D^{(L_1)} = 8$). Note that one-hot encodings are often used linear models, where categorical covariates are coded as dummy variables, and this is a special case where the embeddings are one dimensional. Then, the embedding $h_{r[s]}^{(L_1)}$ for the level 1 ecoregion r containing route s is therefore a vector with $D^{(L_1)}$ elements, given by:

$$h_{r[s]}^{(L_1)} = W^{(L_1)} x_{r[s]}^{(L_1)},$$

which essentially corresponds to extracting column r from the embedding matrix $W^{(L_1)}$.

Embeddings for route s are concatenated with the numeric route-level features x_s (a vector containing climate principal components, road density, distance from coast, latitude, and longitude) to obtain a vector for route s that is the zeroth hidden layer of the neural network $h_s^{(0)}$:

$$h_s^{(0)} = \begin{bmatrix} h_{r[s]}^{(L_1)} \\ x_s \end{bmatrix}.$$

This vector $h_s^{(0)}$ is mapped to next hidden layer with $D^{(1)} = 4$ hidden units via a fully-connected layer, followed by leaky rectified linear unit activation functions (Xu *et al.* 2015). The leaky rectified linear unit activation function is $g(x) = \max(0, x) - 0.01 \times \min(0, x)$. Thus, the next hidden layer is obtained in a forward pass via:

$$h_s = g(W^{(1)} h_s^{(0)}),$$

where $W^{(1)}$ is a $D^{(1)} \times D^{(0)}$ weight matrix. For the single species models, $D^{(0)} = 21$, because there is one embedding of size 8, and an additional 13 elements in the route-level covariate vector x_s (eight principal component axes, elevation, road density, distance from coast, latitude, and longitude).

The hidden layer is then mapped to initial occupancy, persistence, colonization, and detection probabilities, via fully connected layers:

$$\begin{aligned} \text{logit}(\psi_{s,t=1}) &= W^{(\psi_1)} h_s, \\ \text{logit}(\gamma_s) &= W^{(\gamma)} h_s, \\ \text{logit}(\phi_s) &= W^{(\phi)} h_s, \\ \text{logit}(p_{t,s}) &= W^{(p)} (h_s, x_{t,s}^{(p)})' \quad \text{for } t = 1, ..., T. \end{aligned}$$

Here $W^{(\psi_1)}$, $W^{(\gamma)}$, and $W^{(\phi)}$ are 4×1 weight matrices, and $W^{(p)}$ is a $(4 + n_p) \times 1$ weight matrix that maps the concatenation of detection-related hidden unit vector $h_s^{(p)}$ with n_p survey specific features contained in the vector $x_{t,s}^{(p)}$ to the detection probability $p_{t,s}$.

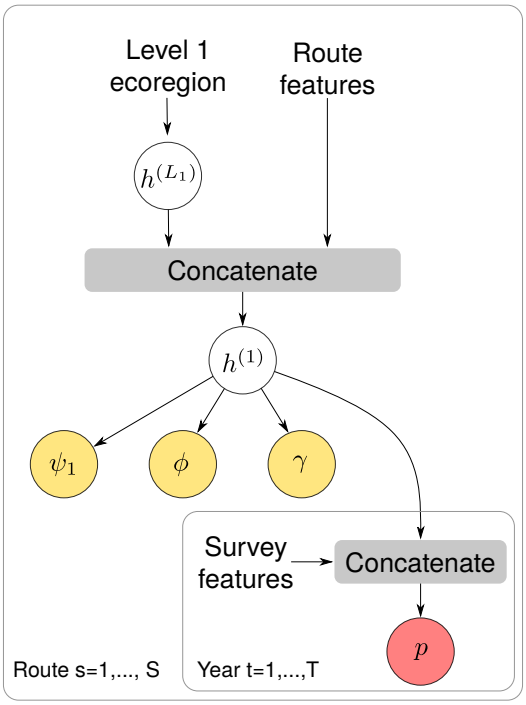

Figure S1: Extended computational diagram for the single species neural dynamic occupancy model. Outer grey boxes indicate the different levels of the model (route and year) that index quantities inside the boxes. Yellow nodes indicate occupancy parameters, and red nodes indicate detection parameters. Hidden layers are represented by h, with layer-specific superscripts. Outputs include initial occupancy (ψ_1), persistence (ϕ), colonization (γ), and detection probabilities (p).

Multi-species neural hierarchical model structure

Presence/absence states $z_{t,s,j}$ for all s, t, and j are equal to 0 if species j is absent from route s in time t, and $z_{t,s,j} = 1$ if the species is present. Occupancy dynamics are modeled as a function of initial occupancy, persistence, and colonization probabilities (Royle & Kéry 2007):

$$z_{t=1,s,j} \sim \text{Bernoulli}(\psi_{t=1,s,j}),$$

$$z_{t,s,j} \sim \text{Bernoulli}(\phi_{t-1,s,j} z_{t-1,s,j} + \gamma_{t-1,s,j}(1 - z_{t-1,s,j})), \quad \text{for } t = 2, ..., T,$$

where $\psi_{t,s,j}$ is the probability of occurrence of species j at route s in year t, $\phi_{t-1,s,j}$ is the probability of persistence conditional on presence in the previous year, and $\gamma_{t-1,s,,j}$ is the probability of colonization conditional on absence in the previous year.

The observations $y_{t,s,j}$ are integer-valued counts in the set $0, 1, 2, ..., 50$ that indicate the number of stops for which species j was detected in year t on route s. Detection/non-detection data are modeled as binomial random variables:

$$y_{t,s,j} \sim \text{Binomial}(z_{t,s,j} p_{t,s,j}, 50),$$

for all s, t, and j.

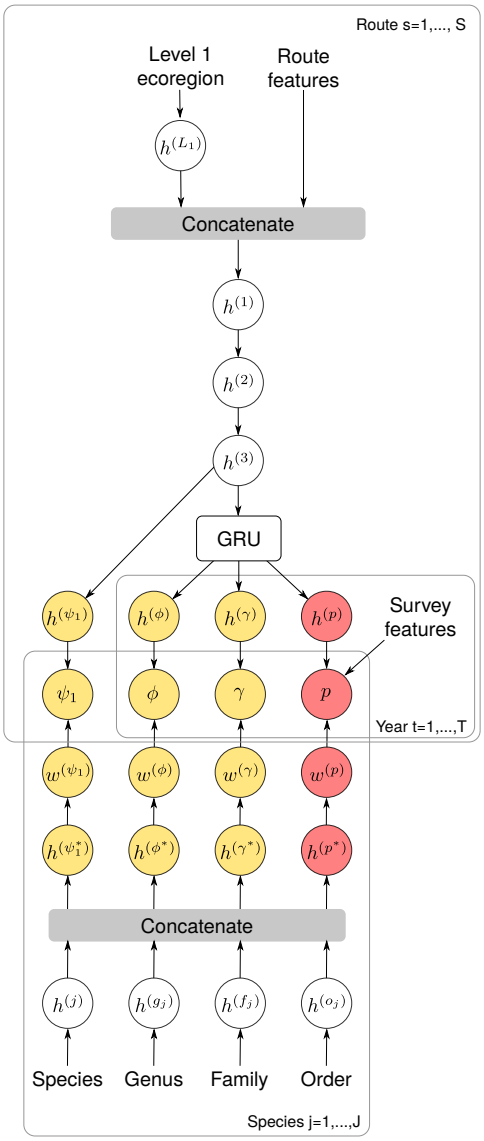

Figure S2: Extended computational diagram for the multi-species neural hierarchical dynamic occupancy model. Outer grey boxes indicate the different levels of the model that index quantities inside the boxes. Yellow nodes indicate occupancy parameters, and red nodes indicate detection parameters. Outputs include initial occupancy (ψ_1), persistence (ϕ), colonization (γ), and detection probabilities (p). The box labeled GRU is a gated recurrent unit that decodes temporal sequences of hidden layers from encoded route vectors.

Route embeddings

Heterogeneity in occupancy dynamics was introduced by allowing species initial colonization, persistence, colonization, and detection probabilities to relate to latent spatiotemporal features (Fig. S2). For the multi-species model, all embeddings are 64 dimensional, all hidden layers are 32 dimensional unless stated otherwise.

Categorical inputs to the network included EPA level one ecoregion, mapped to categorical entity embeddings (Guo & Berkhahn 2016). As with the single-species models:

$$h_{r[s]}^{(L_1)} = W^{(L_1)} x_{r[s]}^{(L_1)},$$

where $h_{r[s]}^{(L_1)}$ is the embedding for a level one ecoregion r containing route s, $W^{(L_1)}$ is a weight matrix, and $x_{r[s]}^{(L_1)}$ is a one-hot encoding for the level one ecoregion r containing route s. Concatenating the ecoregion embedding with route level features x_s for route s provides the zeroth hidden layer of the network.

$$h_s^{(0)} = \begin{bmatrix} h_{r[s]}^{(L_1)} \\ x_s \end{bmatrix}.$$

This is then passed to a sequence of hidden layers:

$$h_s^{(1)} = g(W^{(1)} h_s^{(0)}),$$

$$h_s^{(2)} = g(W^{(2)} h_s^{(1)}),$$

$$h_s^{(3)} = g(W^{(3)} h_s^{(2)}),$$

where g is the leaky ReLU activation function, so that $h_s^{(3)}$ is a vector valued nonlinear combination of route-level features.

This hidden layer is then mapped to parameter-specific hidden layers. The initial occupancy probability hidden layer uses a fully connected layer:

$$h_s^{(\psi_1)} = g(W^{(\psi_1)} h_s^{(3)}).$$

Colonization, persistence, and detection probability hidden layers were allowed to vary in space and time and modeled using a recurrent neural network. Temporal variation was modeled by treating $h_s^{(3)}$ as a route-level encoding, that is decoded by a two-layer gated recurrent unit – a particular type of sequence model often used in time series analysis and text modeling, similar to a long short term memory model (Chung *et al.* 2014). The gated recurrent unit takes the vector $h_s^{(3)}$ as an input, and outputs a multivariate sequence of shape $T \times (32 \times 3)$, which is reshaped into a $T \times 32 \times 3$ dimensional array that has dimensions for years, hidden features, and model components (persistence, colonization, and detection).

$$\begin{bmatrix} h_{1:T}^{(\phi)} \\ h_{1:T}^{(\gamma)} \\ h_{1:T}^{(p)} \end{bmatrix}_s = \text{GRU}(h_s^{(3)}),$$

where the subscript $1:T$ indicates that values are generated for timesteps $t = 1, ..., T$. These latent spatiotemporal route features are then combined with species-specific weights generated via deep multi-species embedding (Chen *et al.* 2016).

Hierarchical deep multi-species embedding

Species-specific weights were modeled as outputs of a neural network that ingests species-level traits (in this case, species identity, genus, family, and order). Taxonomic embeddings enable information to be shared among species within genera, families, and orders. A vector valued embedding v_j for species j is generated by concatenating embeddings at each taxonomic level:

$$
\begin{aligned}
h_j &= W^{(\text{Species})} x_j, \\
h_j^{(g)} &= W^{(\text{Genus})} x_j^{(g)}, \\
h_j^{(f)} &= W^{(\text{Family})} x_j^{(f)}, \\
h_j^{(o)} &= W^{(\text{Order})} x_j^{(o)},
\end{aligned}
$$

$$
v_j = \begin{bmatrix} h_j \\ h_j^{(g)} \\ h_j^{(f)} \\ h_j^{(o)} \end{bmatrix}.
$$

Here h_j is the vector valued embedding for species j, $W^{(\text{Species})}$ is a weight matrix, x_j is a one hot encoded vector, $h_j^{(g)}$ is the vector valued embedding for the genus containing species j, etc. The vector v_j is mapped to parameter-specific hidden units via fully connected layers:

$$
\begin{aligned}
h_j^{(\psi_1^*)} &= g(W^{(\psi_1^*)} v_j), \\
h_j^{(\phi^*)} &= g(W^{(\phi^*)} v_j), \\
h_j^{(\gamma^*)} &= g(W^{(\gamma^*)} v_j), \\
h_j^{(p^*)} &= g(W^{(p^*)} v_j).
\end{aligned}
$$

These hidden layers are then mapped to species-specific weights via fully connected layers with identity activation functions:

$$
\begin{aligned}
w_j^{(\psi_1)} &= W^{(w_{\psi_1})} h_j^{(\psi_1^*)}, \\
w_j^{(\phi)} &= W^{(w_\phi)} h_j^{(\phi^*)}, \\
w_j^{(\gamma)} &= W^{(w_\gamma)} h_j^{(\gamma^*)}, \\
w_j^{(p)} &= W^{(w_p)} h_j^{(p^*)}.
\end{aligned}
$$

By modeling weights as outputs of a neural network with shared features, relationships among weights for occupancy and detection parameters can be learned. By including features (embeddings) at multiple taxonomic levels, information among taxonomically similar species can be shared.

Combining route features and species-specific weights

A dot product combines latent spatiotemporal route features with species-specific weights:

$$
\begin{aligned}
\text{logit}(\psi_{t=1,s,j}) &= h_s^{(\psi_1^*)} \cdot w_j^{(\psi_1)}, \\
\text{logit}(\phi_{t,s,j}) &= h_{t,s}^{(\phi^*)} \cdot w_j^{(\phi)}, \\
\text{logit}(\gamma_{t,s,j}) &= h_{t,s}^{(\gamma^*)} \cdot w_j^{(\gamma)}, \\
\text{logit}(p_{t,s,j}) &= h_{t,s}^{(p^*)} \cdot w_j^{(p)},
\end{aligned}
$$

where $x \cdot y$ is the dot product of x and y: $x \cdot y = \sum_i x_i y_i$.

Implementation

Maximum *a posteriori* estimates of baseline model parameters were obtained with Stan (Carpenter *et al.* 2017; Stan Development Team 2018). Penalized maximum likelihood estimates of the neural hierarchical model were obtained with Pytorch (Paszke *et al.* 2017), with L2 regularization penalties on the network weights, which is equivalent to maximum a posteriori estimation for the neural network with Gaussian priors for the weights (Blundell *et al.* 2015). The discrete latent occupancy states were marginalized using the forward algorithm, so that the optimization objective used the observed data likelihood (rather than the complete data likelihood). To avoid underflow, forward probabilities were computed on the log scale for the baseline model in Stan, and using forward probability scaling in Pytorch for the neural hierarchical models (Rabiner 1989). All code required to reproduce the analysis is available on GitHub at https://www.github.com/mbjoseph/neuralecology.